ADVANCED MATERIALS
www.advmat.de

Recent Advances in Materials, Devices, and Systems for Neural Interfaces

*Sang Min Won, Enming Song, Jianing Zhao, Jinghua Li, Jonathan Rivnay, and John A. Rogers**

Technologies capable of establishing intimate, long-lived optical/electrical interfaces to neural systems will play critical roles in neuroscience research and in the development of nonpharmacological treatments for neurological disorders. The development of high-density interfaces to 3D populations of neurons across entire tissue systems in living animals, including human subjects, represents a grand challenge for the field, where advanced biocompatible materials and engineered structures for electrodes and light emitters will be essential. This review summarizes recent progress in these directions, with an emphasis on the most promising demonstrated concepts, materials, devices, and systems. The article begins with an overview of electrode materials with enhanced electrical and/or mechanical performance, in forms ranging from planar films, to micro/nanostructured surfaces, to 3D porous frameworks and soft composites. Subsequent sections highlight integration with active materials and components for multiplexed addressing, local amplification, wireless data transmission, and power harvesting, with multimodal operation in soft, shape-conformal systems. These advances establish the foundations for scalable architectures in optical/electrical neural interfaces of the future, where a blurring of the lines between biotic and abiotic systems will catalyze profound progress in neuroscience research and in human health/well-being.

1. Introduction

Advances in neural interface technologies and associated experimental methodologies have led directly to many fundamental scientific insights into the function of the central and peripheral nervous systems. Similarly, progress in electrical/optical platforms for such interfaces has followed from the development of materials for devices that can intimately couple electrical/optical functionality with biological systems. Sophisticated platforms are now available, with utility not only in neuroscience research but also in nonpharmacological approaches to treating disease. As examples of the latter, the US Food and Drug Administration has approved a range of implantable neural interface systems for treating diverse neurological disorders, including Parkinson's disease, essential tremor, blindness, and depression.[1–4] The future lies the development of foundational materials for large-scale, high-density platforms with capabilities for measuring and modulating the activity of large neural systems, at the single neuron level and across large, 3D volumes. Mechanically compliant architectures, bioinert constituent materials, and long-lived biofluid barriers represent critical features for stable, chronic operation of such systems in living organisms.

The most widely used technologies exploit various forms of micromanufactured penetrating pins and probes, partly due to their technological maturity and commercial availability, where electrical recording and stimulation occurs via conventional metal electrodes and physical fixturing relies on sutures or surgical glues.[4–6] Electrical impedance and charge injection capacities are of paramount importance, but the materials and structures must also maintain high-quality biological interfaces over long periods of time and support designs that can scale to high-resolution, large-scale collections

S. M. Won
Department of Electrical and Computer Engineering
Frederick Seitz Materials Research Laboratory
University of Illinois at Urbana Champaign
Urbana, IL 61801, USA

Dr. E. Song, Dr. J. Li
Department of Materials Science and Engineering
Frederick Seitz Materials Research Laboratory
University of Illinois at Urbana Champaign
Northwestern University
Evanston, IL 60208, USA

J. Zhao
Department of Mechanical Science and Engineering
Frederick Seitz Materials Research Laboratory
University of Illinois at Urbana Champaign
Urbana, IL 61801, USA

Prof. J. Rivnay
Department of Biomedical Engineering
Simpson Querrey Institute for Nanobiotechnology
Northwestern University
Evanston, IL 60208, USA

Prof. J. A. Rogers
Center for Bio-Integrated Electronics
Department of Materials Science and Engineering, Biomedical Engineering, Chemistry, Mechanical Engineering,
Electrical Engineering and Computer Science, and Neurological Surgery
Simpson Querrey Institute for Nano/biotechnology
McCormick School of Engineering and Feinberg School of Medicine
Northwestern University
Evanston, IL 60208, USA
E-mail: jrogers@northwestern.edu

DOI: 10.1002/adma.201800534

of measurement/stimulation points. The latter requirement demands not only bioinert chemistries but also soft physical properties and curvilinear geometries to match those of neural tissues; the former necessitates use of distributed, active electronic functionality coupled to each electrode site. The goal, then, is for tissue-like, multifunctional electronic/optoelectronic platforms with interfaces that impose zero constraints on the natural dynamic motions of the organs and induce no foreign-body immune responses. In addition to the many challenges associated with developing the necessary active materials, devices, and systems, the platforms must also incorporate defect-free barrier layers to prevent biofluid penetration over timescales that can, for chronic implants, extend to many decades.

The following summarizes results of the latest activities in the field, with an emphasis on findings that have the potential to serve as important foundations for future progress. The review begins with a discussion of electrode materials, including separate consideration of the influence of chemical composition, form, and engineered structure. Following sections highlight the use of these materials in systems with some combination of unique features in scalable interfaces, geometrical configurations, and modes of functional operation. Examples of use with biological systems, from single neurons to large-scale tissues in live animal models, highlight the broad range of advanced capabilities that are now available, as well as the remaining shortcomings of these platforms. Additional sections on bioresorbable technologies and on optoelectronic, microfluidic, and piezoelectric systems highlight some unusual, emerging directions with potential for the development of multifunctional neural interfaces. A concluding section summarizes the state of the field and suggests some opportunities for future research.

2. Neural Interfaces

Fundamentally, neural interface technologies provide means for integrating electronic and/or optoelectronic devices with the central and peripheral nervous system, to enable capabilities in recording, stimulating, and/or inhibiting neural activity. The materials selections for such platforms are critically important as they define the performance and the chronic viability of the interface. For electrical functionality, the electrode/electrolyte boundary can involve either electrochemical reactions (Faradic) or double-layer charging events (capacitive).[4,7–10] The key metrics for sensing and stimulation are impedance (typically at 1 kHz) and charge injection capacity, respectively, where the latter determines the maximum deliverable charge per unit area before irreversible electrochemical reactions occur. Many recent innovations in materials for these purposes, often with attention to form factors (shapes, thicknesses, weight, etc.) and mechanical properties, enable high-performance interfaces with stable operation over long timeframes. The following subsections provide an overview, starting with the base materials themselves, followed by discussions of their forms and of engineering structures built with them, all with an emphasis on key attributes that determine the nature of the biotic/abiotic interface.

Sang Min Won received his B.S. (2009) and M.S. (2011) degrees from the department of Electrical and Computer Engineering from the University of Illinois at Urbana–Champaign. After graduation, he worked for SK Hynix Co., LTD (2011–2014), and involved the development of 30 nm dynamic random-access memory (DRAM) products as a member of team. He is currently a Ph.D candidate under the guidance of Professor John A. Rogers at University of Illinois at Urbana Champaign.

Jonathan Rivnay earned his B.S. (2006) from Cornell University, and his M.S. (2010) and Ph.D. (2012) from Stanford University in Materials Science and Engineering. In 2012, he joined the Department of Bioelectronics at the École Nationale Supérieure des Mines de Saint-Étienne in France as a Marie Curie post-doctoral fellow, working on conducting polymer based devices for bioelectronics. Jonathan spent 2015–2016 as a member of the research staff in the Printed Electronics group at the Palo Alto Research Center (PARC, a Xerox company) before joining the Department of Biomedical Engineering at Northwestern University as an Assistant Professor in 2017.

John A. Rogers obtained B.A. and B.S. degrees in chemistry and in physics from the University of Texas, Austin, in 1989. From MIT, he received S.M. degrees in physics and in chemistry in 1992 and a Ph.D. in physical chemistry in 1995. He spent thirteen years on the faculty at University of Illinois, most recently as the Swanlund Chair Professor and Director of the Seitz Materials Research Laboratory. In 2016, he joined Northwestern University as the Louis Simpson and Kimberly Querrey Professor of Materials Science and Engineering, Biomedical Engineering and Medicine, with affiliate appointments in Mechanical Engineering, Electrical and Computer Engineering and Chemistry.

2.1. Materials

Noble metals (platinum (Pt), iridium (Ir), gold (Au), etc.) and their alloys have, for nearly 50 years, been the most popular choices for neural interface electrodes due to their chemically

inert nature, biocompatibility, and good electrical properties in biological environments.[9–12] The relatively high impedances and limited charge storage capacities associated with these materials, however, represent key limitations that increase in significance as the electrode sizes decrease to support improved spatial resolution.[12–15] Planar microelectrodes of Pt have impedances of ≈1 MΩ (measured at 1 kHz for circular electrodes with area of 3×10^2 μm^2), with associated noise levels (≈100 μV) that create challenges in neural sensing when signal levels fall below 100 μV (e.g., 50–100 μV for electrocorticography (ECoG), 10–20 μV for electroencephalography, and ≈1 μV for evoked potential[16,17]).[14] Such Pt electrodes also have limited charge injection limits, typically between 50 and 150 μC cm^{-2},[7] thereby frustrating reliable stimulation of tissues such as the retinas of visually impaired patients, where the thresholds are typically 50–350 μC cm^{-2}.[18–20] By comparison, electrodes formed with sputtered iridium oxide offer relatively high charge capacities (1–5 mC cm^{-2})[7] due to charge injection via reversible Faradaic reactions involving reduction and oxidation between the Ir^{3+} and Ir^{4+} oxide states.[11,21,22] Capacitive charging interfaces with similar performance are possible with sputtered titanium nitride (TiN) (≈1 mC cm^{-2}) owing to its high surface roughness.[7] In this case, as with all material choices, increasing the effective surface area by the addition of random or engineered roughness and porosity reduces the electrochemical impedance and improves the charge injection capacity, as described subsequently.

Conductive polymers (CPs), often electropolymerized directly onto standard metal electrodes, offer nanotextured, porous surfaces, together with a mixed electronic/ionic transport in the bulk and volumetric charging,[7,23] resulting in high charge capacity and low impedance. Synthetic flexibility and diversity in processing modalities allow for tunable ionic/electronic transport properties and biochemical surface functionalization, with consequences in improved electrode/device performance and longevity on operation.[6] Poly(3,4-ethylenedioxythiophene) (PEDOT), doped with poly(styrene sulfonate) (PSS), represents a popular class of CP due to its chemical stability and relatively high conductivity (>300 S cm^{-1}).[24–26] The impedance can reach 100 kΩ at 1 kHz for an electrode area of 3×10^2 μm^2, corresponding to an order of magnitude reduction compared to Pt, with significant improvements in signal-to-noise ratios in neural recordings.[14] Adding nerve growth factors or peptides to PEDOT:PSS can improve biological interactions, cell adhesion, and neuronal growth, thereby further increasing the biocompatibility and signal fidelity.[27,28] Furthermore, PEDOT:PSS, as deposited onto Au electrodes, can support charge injection capacities of ≈15 mC cm^{-2}, which is roughly three times higher than that of iridium oxide.[7] One challenge is that interactions between the polymer coating and the underlying noble metal electrodes are often weak,[29–32] leading to delamination under chronic implantation in vivo.[33,34] Recent efforts suggest that wet chemical deposition of porous layers of Pt on top of smooth Pt electrodes can significantly improve the adhesion, to avoid delamination of PEDOT coatings for more than ≈100 d in accelerated aging tests (phosphate-buffered-saline (PBS) solution at 60 °C), corresponding to a factor of five improvement compared to the native Pt surface without modification.[30] In other approaches, surface functionalization with (2,3-dihydrothieno[3,4-b][1,4] dioxin-2-yl)methanamine (EDOT-NH_2) can lead to strong covalent bonding between PEDOT and planar electrodes, as demonstrated by robustness against delamination even during ultrasonication for up to an hour (compared to 5 s without modification).[35]

Other materials of recent interest include nanoscale forms of carbon such as graphene and carbon nanotubes (CNTs) due to their excellent electrical and thermal conductivity, chemical stability, mechanical strength, low density, high surface area, and wide electrochemical window.[36] These characteristics also lead to low impedances and high charge capacities.[37,38] Careful measurements indicate that the impedances of microelectrode arrays formed with CNT–Au nanocomposites (1 kHz impedance of 50 kΩ with area of 176 μm^2) are tenfold smaller than those of otherwise similar electrodes without the CNTs.[39] The high geometrical surface areas associated with the nanotube structure result in charge capacities of 1–1.6 mC cm^{-2},[7] as reported from vertically aligned nanotube electrodes. CNT fibers with site surface areas of 1450 μm^2 also show improved impedance values, 15-fold lower than those of PtIr wires with the same dimensions. These enhancements follow from the accessibility of ions to interstitial spaces between the aligned CNTs that form the fiber.[40] The main disadvantage of CNTs relates to their potential biotoxicity.[12] Graphene, by contrast, largely bypasses this concern due to its planar, sheet-like geometry. As a replacement for traditional electrodes, graphene is attractive due to its high conductivity and relatively low toxicity, and its transparency for simultaneous electrophysical recording, neural imaging, and optogenetics, as further elaborated in Section 3.4. Good biocompatibility, as evidenced by in vitro studies of neural cell culturing,[41,42] leads to enhanced adhesion and viability. In vivo biodistribution and cytotoxicity of graphene-based nanomaterials depend on the dose, the routes for administration, and on surface chemistry[43–49] For example, graphene functionalized with polyethylene glycol (PEG) intravenously injected into mice for 3 months does not induce appreciable toxicity at doses of 20 mg kg^{-1} as evidenced by blood biochemistry, hematology, and histology analysis.[47] Intraperitoneal injections of graphene oxide and PEGylated graphene oxide at doses of 50 mg kg^{-1} also shows insignificant toxicity despite the long-term retention (>1 month) in the body.[48] Another report, however, suggests toxicity of intravenous injected graphene oxide with doses of more than 50 μg mL^{-1}.[49] The electrochemical properties of graphene are similar to those of Pt and Au, and the charge capacities for planar, nonstructured graphene formed by chemical vapor deposition (CVD) are between 5 and 20 μC cm^{-2}.[50] The performance of graphene-based recording electrodes can be significantly improved by engineering the structure to increase the surface area,[51] as outlined in Section 2.2. As a result, structured graphene-based materials and composites represent promising candidates for future neural interfaces.

Doped semiconductors also have utility as electrode materials, with the additional advantage that they can support capabilities in local, per-channel signal amplification and multiplexing,[52–56] molecular-scale communication with cells,[57–59] and compliant, bioresorbable mechanics in vivo.[60]

In one example, semiconductors serve as the active channel materials in field-effect transistors (FETs) that provide sensing capabilities as a result of changes in conductance induced by local changes in the field due to fluctuating biopotentials, with straightforward options in multiplexed readout of measured signals. Here, the sensitivity scales with the ratio of the width to the length of the channel region instead of the sensing area, thereby allowing measurements at the molecular scale. In addition, the intrinsic amplification provided by the FETs can reduce the significance of external noise.[52–59] This type of operation can be achieved with various materials including silicon,[53,54,57,58] graphene,[55,56] CNTs,[52] and organic electrochemical transistors (OECT) with PEDOT:PSS as the gate electrode and channel material for integrated amplification of biosignals.[61,62] Numerous publications describe the use of silicon nanowire FETs, as outlined in a subsequent section, in a range of interface structures including 3D nanoscale probes (i.e., kinked silicon nanowires),[58] scaffolds,[63] and mesh-like configurations.[64,65] Demonstrations show capabilities in recording of intracellular activity in cardiomyocytes and extracellular action potentials at the single-neuron level. In other reports, highly doped monocrystalline silicon nanomembranes (Si NMs; phosphorous at $\approx 10^{20}$ cm^{-3}) serve as electrodes with impedance (≈100 kΩ at 1 kHz for area of 4×10^4 μm^2) comparable to that of Au electrodes (≈30 kΩ at 1 kHz) in the same size regime.[60] The results form the basis of stable neural recording electrodes that are ultimately bioresorbable by hydrolysis ($Si + 4H_2O \rightarrow Si(OH)_4 + 2H_2$) in biofluids, as summarized in detail in Section 3.3.

2.2. Material Forms

As in the case of surface texture, material form factors are critically important in defining not only the electrical performance and the biochemical stability, but also in creating extended applications in intracelllular recording/stimulation, at the individual neuron scale, with enhanced adhesion to biotissues. Widely explored examples involve the use of coatings of nanoparticles, nanowire, and porous materials on otherwise conventional, planar electrodes. Such approaches are attractive for improving the impedance properties of dense, inorganic materials where charge accumulation or desired reactions are defined by the effective surface area of the electrolyte–material interface. **Figure 1**a shows the case of Au nanoparticles (Au NP) deposited on a Au electrode using a layer-by-layer assembly technique.[66] This modification in form factor improves the charge storage capacity to 2.56 mC cm^{-2}, corresponding to a fourfold increase over the bare Au electrode (0.4–0.6 mC cm^{-2}).[67,68] For electrodes with sizes of 7×10^2 μm^2, the impedance (200 kΩ at 1 kHz) decreases by a factor of 3.[69] Similarly, electroplating form of Pt that includes nanoparticulate-like features, commonly known as Pt black, reduces the impedance by fivefold (from 16.6 to 3.5 kΩ at 1 kHz) and enhances the charge injection capacity by more than eightfold (from 0.286 to 1.906 mC cm^{-2}) by increasing the effective surface area, as reported for the case of interfaces formed on the tips (75 μm diameter) of tungsten (W) microelectrode wires.[70]

Compared to nanoparticles, nanowires and nanorods offer not only enhanced surface areas but also improved ability for electrical addressing. As an example of the former, decorating an electrode surface with Au nanorods (70 nm in diameter and 500 nm in length) (Figure 1b) leads to a 25-fold decrease in the interface impedance (1.847 kΩ at 1 kHz compared to 45.24 kΩ of planar Au electrode with area of 10^4 μm^2), roughly consistent with the corresponding increase in areas.[71] As an example of the latter, nanowires can probe directly into the depths of tissues and/or into intracellular spaces. Figure 1c shows an array of vertically oriented silicon nanowires (≈150 nm in diameter and 3 μm in length) coated with titanium (Ti) and Au on their tip ends as platforms for intracellular recording and stimulation with single cellular resolution.[72] Nanoscale FETs integrated at the tips of kinked silicon nanowires (Figure 1d) can also capture intracellular potentials. Probes of this type exhibit conductance sensitivity of 4 to 8 μS V^{-1} and pH sensitivity (≈58 mV pH^{-1}) near the Nernstian limit.[58] Arrays of silicon nanowire FETs enable simultaneous measurement of the rate, amplitude, and shape of signals propagating along individual neuron cells that are guided to grow with a good alignment on prefabricated arrays of silicon nanowire FETs.[57] Additional details on silicon nanowire FETs as neural interfaces are reviewed elsewhere.[59]

Materials in porous forms combine certain attributes of particulates and wires, but with an additional capability in providing structural scaffolds and 3D-distributed interfaces with utility not only in neural recording/stimulation but also in tissue engineering. Figure 1e shows a 3D porous graphene structure produced by direct laser pyrolysis of a polyimide substrate. This type of electrode (9×10^4 μm^2) has an impedance approximately two orders of magnitude smaller than a Au electrode with similar size.[51] The corresponding charge injection capacity (≈3 mC cm^{-2}) is two orders of magnitude higher than that of a planar, unstructured graphene electrode (5–20 μC cm^{-2}).[50] In the field of tissue engineering, these porous structures support cell growth and provide tailored 3D microenvironments. For example, porous graphene scaffolds and laser micropatterned PEDOT:PSS increase the proliferation of neural stem cells and adhesion of electrogenic cells respectively, compared to planar counterparts.[73,74] Microelectrodes with nanostructured porous surfaces studies in vivo also show improved biocompatibility, resulting in increased numbers of neurons and decreased glial activation adjacent to the surfaces of the electrodes compared to the smooth counterpart.[75–77] In both in vitro and in vivo investigations, the porous 3D network generally facilitates proliferation and cell growth, where porosity and pore size affect the behavior of surrounding cells.[78]

Percolating networks of these various forms of materials in soft polymer matrices can yield readily processable composites with attractive electrical attributes and low modulus mechanics for chronic integration with soft tissues. As a specific example, polydimethylsiloxane (PDMS) loaded with Pt nanoparticles (0.5–1.2 μm diameter; Figure 1f) can yield electrodes with impedances (≈4 kΩ at 1 kHz, area of 7×10^4 μm^2) that are one order of magnitude lower than those of bare Au electrodes with similar sizes.[79] The tensile modulus in this particular case is only ≈10 MPa, much smaller than that of conventional metal electrodes (≈GPa) and approaching value

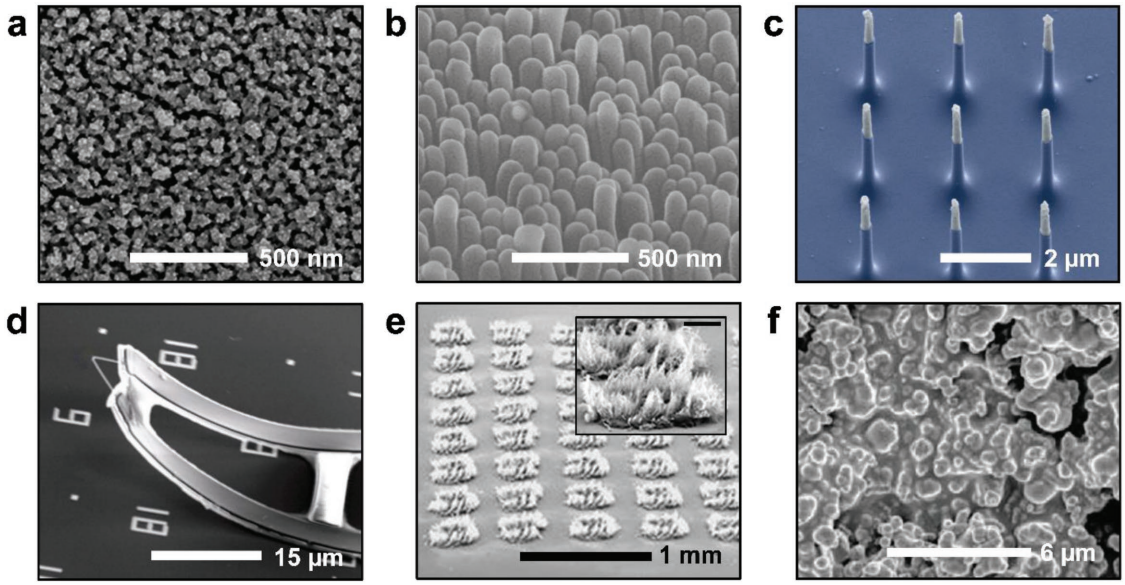

Figure 1. Electrode materials in various forms. a) SEM of layer-by-layer assembled films from Au nanoparticles. Reproduced with permission.[62] Copyright 2012, American Chemical Society. b) SEM of Au nanorod arrays (70 nm in diameter and 500 nm in length) formed by deposition of metal into the pores of porous alumina templates. Reproduced with permission.[71] Copyright 2009, Institute of Electrical and Electronics Engineers. c) SEM of vertically aligned silicon nanowires (≈150 nm in diameter and 3 μm in length) for intracellular recording and stimulation. Each nanowire consists of a silicon core encapsulated by a silicon dioxide, with thin metal films (Ti and Au) on their tip ends. Reproduced with permission.[72] Copyright 2012, Nature Publishing Group. d) SEM of a kinked (60°) silicon nanowire probe integrated with photopatterned epoxy (i.e., SU-8) and metal contacts. Reproduced with permission.[58] Copyright 2009, American Association for the Advancement of Science. e) SEM of porous graphene array formed by direct laser pyrolysis on a polyimide film. The inset provides a magnified scanning electron microscope image of an individual electrode. Scale bar: 100 μm. Reproduced with permission.[51] Copyright 2016, Nature Publishing Group. f) SEM of a percolating network of Pt nanoparticles in a PDMS matrix. Reproduced with permission.[79] Copyright 2015, American Institute of Physics.

characteristic of soft biological tissues (≈kPa). The electrical properties of such systems can be improved by replacing PDMS with a conductive polymer such as PEDOT. Electrodes formed by electrodeposition of PEDOT:PSS mixed with multiwalled carbon nanotubes (area of ≈600 μm^2) exhibit charge injection limits of ≈8 mC cm^{-2} and impedances of ≈10 kΩ at 1 kHz, corresponding to two orders of reduction from bare Au electrodes.[80] Loading sheets of graphene into PEDOT:PSS can also improve the electrical properties, as evidenced by a 41% increase in the electrical conductivity with addition of only 3 wt% of graphene.[81] Advanced composites incorporate biological materials, such as extracellular matrix materials, for enhanced cell adhesion and minimized inflammatory responses, without compromising the mechanics or the electrical properties.[82,83] PEDOT dispersed in a collagen matrix represents an example of this type, where data indicate ability to support growth and proliferation of PC-12 cells and human skeletal muscle cells.[83]

Related composites can also be formed with hydrogels, for further improved mechanical matching between electrodes and tissues. Here, the desired electrical performance can be maintained by exploiting ionic transfer through hydrogel coatings on metal electrodes.[12] Examples of hydrogels include natural materials (i.e., collagen and arginate) or synthetic polymers (i.e., polyvinyl alcohol (PVA), polyethylene glycol, and polyacrylamide). The intrinsic hydrophilic properties of these materials and their high water content provide access of aqueous electrolytes throughout the entire 3D hydrogel matrix, rather than across a 2D planar surface, thereby increasing the charge transfer area.[84] As an example, copolymer hydrogels of PEDOT/PVA coated on Pt electrodes improve the charge injection capacity (0.09–2.42 μC cm^{-2}) by 24 times compared to otherwise similar electrodes without the coating.[85] The elastic moduli of such composite forms of PEDOT/PVA (≈2 MPa) are significantly lower than that of PEDOT itself (≈40 MPa).[86] The result improves interactions at the interface by minimizing mechanical damage to tissues.[87] Embedding living cells into degradable hydrogels represents an interesting method to reduce foreign body responses, where there cells can form a natural matrix scaffold, for a continuous, diffuse boundary between the electrodes and adjacent tissues as the hydrogel degrades.[11,84] Coatings based on hydrogels loaded with immunosuppressant and neurotrophic factors (i.e., nerve growth and brain-derived neurotrophic factors) also improve neuronal integration as demonstrated in vivo, where probes with such coatings exhibit larger numbers of spike activity and increased signal-to-noise ratio compared to noncoated counterparts.[88]

2.3. Engineered Material Structures

Engineering control over the materials and material forms described in the previous sections can enhance long-term stability and biocompatibility through overall miniaturization, addition of coatings at critical interfaces sites, and adoption of configurations that match mechanics and shapes to neural

tissues. Many strategies focus on overcoming intrinsic limitations associated with the material properties of conventional electrodes for noninvasive implantation and subsequent chronic operation, in a way that avoids tissue damage and immune responses.[6,11,89] One specific direction is in the design of composite material structures that provide effective mechanics and geometries tailored to those of the targeted biological interface. **Figure 2** shows a collection of examples, evolving from rigid shanks and micromachined electrodes to flexible, conformable, and mesh-like constructs. Microlithographically defined electrodes in platforms commonly referred to as "Utah arrays" (Figure 2a)[90] and 'Michigan probes' provide examples of early work in this area. Such systems are technically mature and currently serve as some of the most widespread tools for neuroscience research and exploratory clinical work.[6] Utah arrays combine interconnected collections of silicon needles (typically 10×10 or 13×13, each 0.5–1.5 mm in length and 40–100 μm in diameter[91,92]) that localize signals from the corresponding regions of the brain, with a measurement interface that consists of iridium oxide or Pt on highly doped silicon.[93,94] The Michigan probe consists of a single shank (15 μm thick and 50 μm wide[95]) with a linear array of electrodes, typically flat metal pads of Au, Pt, or iridium oxide, distributed along its length.

Active research focuses on further miniaturization of the needles and shanks in related systems to address, in a simultaneous manner, tissue damage associated with device insertion and persistent irritation and glial responses associated with long-term operation. Figure 2b shows an example of a structure that consists of four passive electrodes (500 nm thick layers of Au) embedded in an ultrathin (1.5 μm) and narrow (10 μm) polymer (photodefinable epoxy, SU-8) needle substrate.[96]

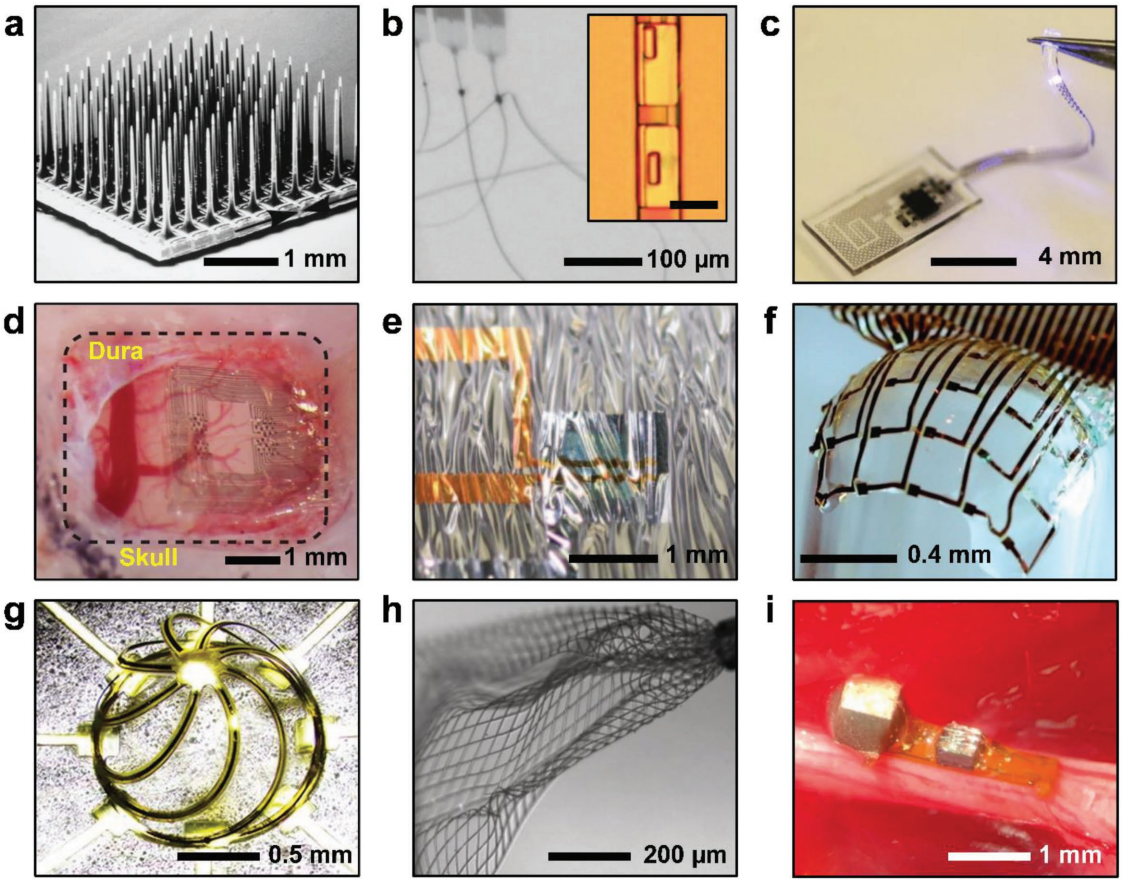

Figure 2. Engineered material structures. a) SEM of Utah Intracortical Electrode Array. Electrode length is 1 mm long with an interelectrode spacing of 400 μm. Reproduced with permission.[90] Copyright 1999, Institute of Electrical and Electronics Engineers. b) Opticam image of ultrathin (1.5 μm) and narrow (10 μm) polymer (photodefinable epoxy, SU-8) needles, consisting four passive Au electrodes. The inset shows an optical image of two electrodes (area of 200 μm^2). Scale bar: 10 μm. Reproduced with permission.[96] Copyright 2017, American Association for the Advancement of Science. c) Photograph of a soft, stretchable optogenetic stimulator consisting thin, serpentine patterned Au films in 100 μm thick PDMS sheet. Reproduced with permission.[113] Copyright 2015, Nature Publishing Group. d) An optical image of ultrathin (4 μm) electrode array placed on the surface of the rat somatosensory cortex for electrophysiology. Reproduced with permission.[116] Copyright 2015, Nature Publishing Group. e) Optical image of an ultrathin, wavy plastic electronic foil on a soft, stretchable silicone substrate. Reproduced with permission.[120] Copyright 2013, Nature Publishing Group. f) Photograph of a passive metal electrode in an open mesh framework wrapped around the hemispheric surface of glass rod. Reproduced with permission.[117] Copyright 2010, Nature Publishing Group. g) Optical image of a 3D scaffold integrated with eight addressable electrodes for stimulation and recording. Reproduced with permission.[123] Copyright 2017, National Academy of Sciences. h) Optical image of macroporous flexible mesh electronics injected into aqueous solution through a syringe. Reproduced with permission.[64] Copyright 2015, Nature Publishing Group. i) Optical image of an ultrasound-based neural interface placed on sciatic nerve in an anesthetized rat. Reproduced with permission.[129] Copyright 2016, Cell Press.

This ultraflexible probe, referred to as a nanoelectronic thread, reduces the effective bending stiffness to 10^{-15} N m^2 (compared to $\approx 10^{-8}$ N m^2 for a stainless microwire with a diameter of 50 μm and $\approx 10^{-9}$ N m^2 for a silicon probe with cross-sectional dimensions of 15 × 60 μm[96]), leading to extremely small interfacial forces, in the nano-Newton range. This ultralow bending stiffness demands a temporary support to provide mechanical stiffness for insertion into the brain. Reports describe the use of a 7 μm diameter carbon fiber for this purpose. Such interface architecture is suitable for chronic recording as demonstrated by operation in the somatosensory and visual cortices for 4 months with stable impedances and noise levels. The same principles of miniaturization also apply to engineered multielectrode fiber probes. In published examples, long, narrow fibers (≈85 μm diameter) made of poly(etherimide) (PEI) embed up to seven TiN electrodes (≈5 μm diameter and ≈23 μm spacing).[97] Such probes have impedances of ≈900 kΩ at 1 kHz with bending stiffnesses of 4–7 N m^{-1}, an order of magnitude lower than that of steel microwires with 125 μm diameter. In vivo demonstrations include electrophysiological studies of the prefrontal cortex of mice, with negligible glial response.

Ultrasmall dimensions and bending stiffnesses in such miniaturized microprobes mechanically preclude their self-supported implantation into the brain. Conventional strategies include temporarily attaching the probe to a rigid shuttle,[98–100] reducing the effective length of the probe with a dissolvable polymer,[101,102] high-speed modes of insertion,[103] and dynamical softening of the probe substrate material after insertion.[104–107] Inspired by the labium guide of the mosquito, a recent alternative utilizes an insertion guide made of poly(methyl methacrylate) on the skull above the site of device implantation.[108] Here, a narrow slit (≈250 μm) provides lateral support and additional bracing (height of 1 mm) prevents buckling. With the guide in place, the critical buckling force of the microprobes (a 3 mm long shank with 200 μm width and 30 μm thickness) increases by nearly four times, resulting in 100% successful insertion into rat motor cortex compared to 37.5% without the guide. This bioinspired strategy provides an additional probe insertion method that can complement other strategies described above, with additional applicability to other types of microscale medical devices.

The mechanics of devices that use polymer substrates can be further improved by the use of thermosets with tunable modulus. As a specific example, thio-ene/acrylate polymer can soften from 1≈2 GPa in the dry state to 10–50 MPa with a small water uptake (≈3% swelling over 4 weeks) at physiological temperatures (37 °C) and aqueous environments.[106,109] PEDOT:PSS electrodes (area of 177 μm^2) on a substrate of this type (2.5 mm long shank with 265 μm width and 35 μm thickness) exhibit impedances of ≈50 kΩ, with stable operation after softening. The probe enables in vivo neural single unit recording from the rat motor cortex for 77 d without mechanical/electrical performance degradation.[109]

Exchanging the polymer (i.e., SU-8, polyimide, and PEI) substrate with a low modulus elastomer yields probes that are not only flexible (i.e., low bending stiffness) but also stretchable (i.e., low modulus, high failure strain), thereby further improving the mechanics and allowing for motions that can follow the natural dynamics of soft tissues in biological systems.[110] Specifically, displacements in the brain and peripheral nerves can correspond to local strains of 5% and 15%,[111,112] respectively, in typical cases and much more in other certain circumstances. As an elastomer for such purposes, PDMS is attractive due to its established biocompatibility and its ability to be formed and patterned into a broad range of geometries by the techniques of soft lithography. Examples of the use of PDMS in this context include neural interfaces to highly mobile areas of the peripheral nervous system and the spinal cord. Figure 2c shows a device where thin, filamentary serpentine structures of Au form interconnects embedded in a sheet of PDMS with a thickness of 100 μm.[113] Here, the effective modulus is 1.7 MPa, comparable to the PDMS itself and four orders of magnitude lower than the Au (79 GPa). The maximum tolerable strain before plastic deformation of the filamentary traces is 40%, corresponding to an improvement of hundreds times over yielding point of Au (0.3%).[114] The electronic dura mater represents another example of an elastomeric system, but in this case one that combines pharmacological delivery with electrical interfaces.[115] Here, Au interconnects, Pt–silicone composite electrodes, and fluidic microchannels integrate into a soft silicone substrate, resulting in an effective modulus of 1.2 MPa and maximum tolerable strain up to 45%. Deployment in the spine of an awake, moving rodent can restore locomotion in a paralyzed animal through both pharmacological and electrical activation in the subdural space. These attractive mechanical properties allow the devices to accommodate a broad range of anatomical shapes and natural motions.[113,115]

Ultrathin electrode arrays in sheet-like geometries can exploit related mechanics principles for flexible neural systems that can conform to the dynamic, curved surface of the brain in ultrahigh-resolution ECoG.[53,116,117] Here, the thin construction yields bending stiffnesses sufficiently small for conformal contact, thereby reducing the effective impedance and enabling recording over large areas.[118] In one example, an ultrathin substrate of parylene (4 μm thickness) supports (Figure 2d) Au interconnects and an array of PEDOT:PSS-based sensing electrodes (100 μm^2).[116] One embodiment includes 256 electrode sites, capable of recording both local field and action potentials from superficial cortical layers of rodents over 10 d without signal deterioration. Initial studies also validate operation in human epileptic patients.

Advanced approaches exploit bending mechanics to define "wavy" structures by controlled buckling processes on the surfaces of soft elastomers. The resulting systems are not only flexible but also stretchable, even in device designs that include brittle inorganic materials such as Si NMs.[119,120] Figure 2e shows this idea implemented with an array of organic transistors on a wavy polyimide sheet (1 μm thickness) that can be stretched reversibly, with strains up to 230%, without degradation in electrical performance (on-current, mobility, and threshold voltage).[120] This strategy can be applied to a broad range of materials including graphene, silicon, metals, and others.[119,121,122] Forming such structures into open mesh frameworks further enhances the mechanics, as in Figure 2f.[117] A simple demonstration illustrates that a thin polyimide mesh (2.5 μm thick) can conform to the surface of a hemisphere after removal of a temporary, bioresorbable support. In vivo

validation studies on the visual cortex of a feline animal model demonstrate that the amplitudes and accuracies of signals captured using this mesh significantly exceed those of otherwise identical counterparts formed on uniform sheets of polyimide, even at exceptionally small thicknesses (2.5 μm). No evidence of immune responses after 4 weeks suggests enhanced biocompatibility for these mesh designs.

Complex 3D structures with similar open geometries and with dimensions in a mesoscopic range offer a unique combination of biocompatibility, deformable mechanics, and volumetric capabilities for integration with cells. Sensing and activation in 3D can yield important extracellular and intracellular information on growing neural networks.[63,123] Figure 2g demonstrates that electrodes (circular Au with area of 2×10^3 μm^2) in a 3D scaffold can serve as an "instrumented" growth platform for dorsal root ganglion neurons.[123] Data indicate successful stimulation and recording of action potentials after 7 d of culturing. Similar advantages in deformability, biocompatibility, and 3D integration apply to structures formed with Si nanowire FETs or Pt electrodes, as in a thin (1 μm) structure of photodefined epoxy (SU-8) shown in Figure 2h.[64] This type of platform can be delivered into tissue as a floating mesh through a syringe or as a penetrating probe temporarily rigidified by freezing in liquid nitrogen.[64,65] The ultralow bending stiffnesses (≈0.087 nN m) and small feature sizes (5–20 μm) minimize tissue disruption during insertion and tissue responses during chronic use. Studies show that the level of glial fibrillary acidic protein expression is similar with and without the mesh electronics. In other approaches, 2D sheets rolled into 3D cylinders yield related interface systems with additional capabilities in local drug release.[124] The release strategy relies on an electrical stimulation process that protonates and thereby volumetrically shrinks a hydrogel preloaded with protein. This platform enables electrical and therapeutic activation from multiple channels, with simultaneous recording capabilities.

Other designs are also possible. In one approach, a stent-like structure with a Pt electrode (750 μm diameter) enables intracranial neural activity recording from within veins in the brain.[125] This surgical approach, as an established technique in neurosurgery for arterial and venous neurological conditions, qualitatively differs from implantation of subdural, epidural, and penetrating arrays based on invasive, open craniotomies.[125–127] The implantation uses catheter angiography to guide device placement to a desired location of the brain, where the stent expands and attaches to the walls for recording of neural activities. As an example, integration within the superficial cortical vein overlying the motor cortex enables high-fidelity recording of somatosensory evoked potentials in the brain of a sheep for 190 d. This type of platform, particularly in future embodiments that might be enabled by some of the other technology approaches and materials summarized here, could provide a minimally invasive option for deep brain recording. Use for deep brain stimulation will require further investigations of stimulation parameters, safety profiles, and substantial additional studies in vitro and in vivo.

In all of these cases, the neural interfaces require hard wired connections or electromagnetic (EM) interfaces to external electronics for control and data acquisition. For in vivo applications, the former has disadvantages in infection, tissue damage, and physical constraints; the latter has limitations associated with EM penetration and in power supply. For example, recent inductively powered neural stimulators with sub-millimeter scale dimensions (device volume of 0.3–0.5 mm^3) can produce voltages between 100 and 1000 mV depending on the distance and angular rotation of receiver relative to the plane of the power transmitter.[128] Alternative schemes use acoustic coupling, where ultrasonic backscattering from a piezoelectric crystal forms the basis of the process for measuring biopotentials at peripheral nerves.[129] Initial demonstrations of devices of this type (Figure 2i) involve a single transistor (0.5 × 0.45 mm), a piezoelectric transducer (0.75 × 0.75 × 0.75 mm), and Au recording electrodes (0.2 × 0.2 mm). Ultrasonic waves launched from an external source vibrate the transducer, thereby converting the mechanical energy to electrical power to supply the transistor. Biopotentials that appear across the two recording electrodes then modulate the current through the transistor and consequently current to the transducer, thereby altering the vibration and intensity of the reflected ultrasonic energy. Scalable application of such concepts to platforms with sub-millimeter dimensions will require advances in materials and designs for the transducers and in ultrasonic focusing techniques.

3. Neural Interface System Development

The following sections describe recent results in the development of fully integrated systems that exploit the materials, material forms, and/or engineered structures outlined in the preceding sections. The emphasis is on neural interface technologies that embed circuit level functionality in scalable architectures capable of supporting many thousands of channels for neural recording and/or modulation.

3.1. High-Density Neural Interfaces

Interface systems with high spatial and temporal resolution yield powerful capabilities in neuroscience and clinical research. The achievable resolution set by biological considerations strongly depends on the nature of the neural interface (surface or penetrating) and on the animal models, the types of measurements, and the nature of the signal analysis. Based on spatial spectral analysis and finite-element modeling, with single dipole sources, the spatial resolution of subdural ECoG is ≈1 and 0.5 mm for human and rat cortex, respectively.[130,131] Experimental results of Viventi et al. demonstrate μECoG with distinguishable resolution of ≈0.5 mm in a feline model,[45] and Khodagholy et al. observed extracellular action potentials in less than 60 μm resolution from rat and human brain cortex.[61,132] Spatial scales for intracortical signals are ≈0.5 mm for local field potentials, ≈0.1 mm for multiunit activity, and 0.05 mm for single-unit activity.[133,134] Demands for addressing large numbers neurons or collections of neurons, over large areas and at high sampling rates, motivate the development of high-resolution, high channel neural interface systems that leverage high-performance electronics for addressing, amplification, and preprocessing. Since the 1950s, the number of channels in such

systems has doubled every 7 years such that the latest platforms can support thousands of individual recording channels.[135] In this context, an ambitious goal for penetrating shank technologies is dense, distributed interface sites (<30 µm site space) to isolate individual neurons across scalable regions of the brain with excellent resolution.[136] In µECoG devices, high densities currently correspond to $>10^3$ electrodes cm^{-2}, with thousands of amplified and multiplexed independent channels distributed across large regions of the brain (≈10 × 9 mm), and minimal numbers of independent external connections.[53,137] Combined advances in electrode materials, electrode addressing electronics, and overall systems designs underpin this progress, where overall form factors range from planar arrays to micromachined collections of penetrating electrodes to flexible, multichannel filaments.

In planar formats, lithographic processes and other semiconductor manufacturing techniques adapted from those used in the integrated circuit industry can be leveraged directly.[130,131] **Figure 3**a shows a system based on a 130 nm CMOS fabrication process that yields sophisticated electronics for multiplexed addressing and local amplification from 960 recording electrodes placed on a single, 10 mm long, rigid shank with a cross section of 70 × 20 µm, formed by micromachining from the original silicon wafer substrate.[136] The interface

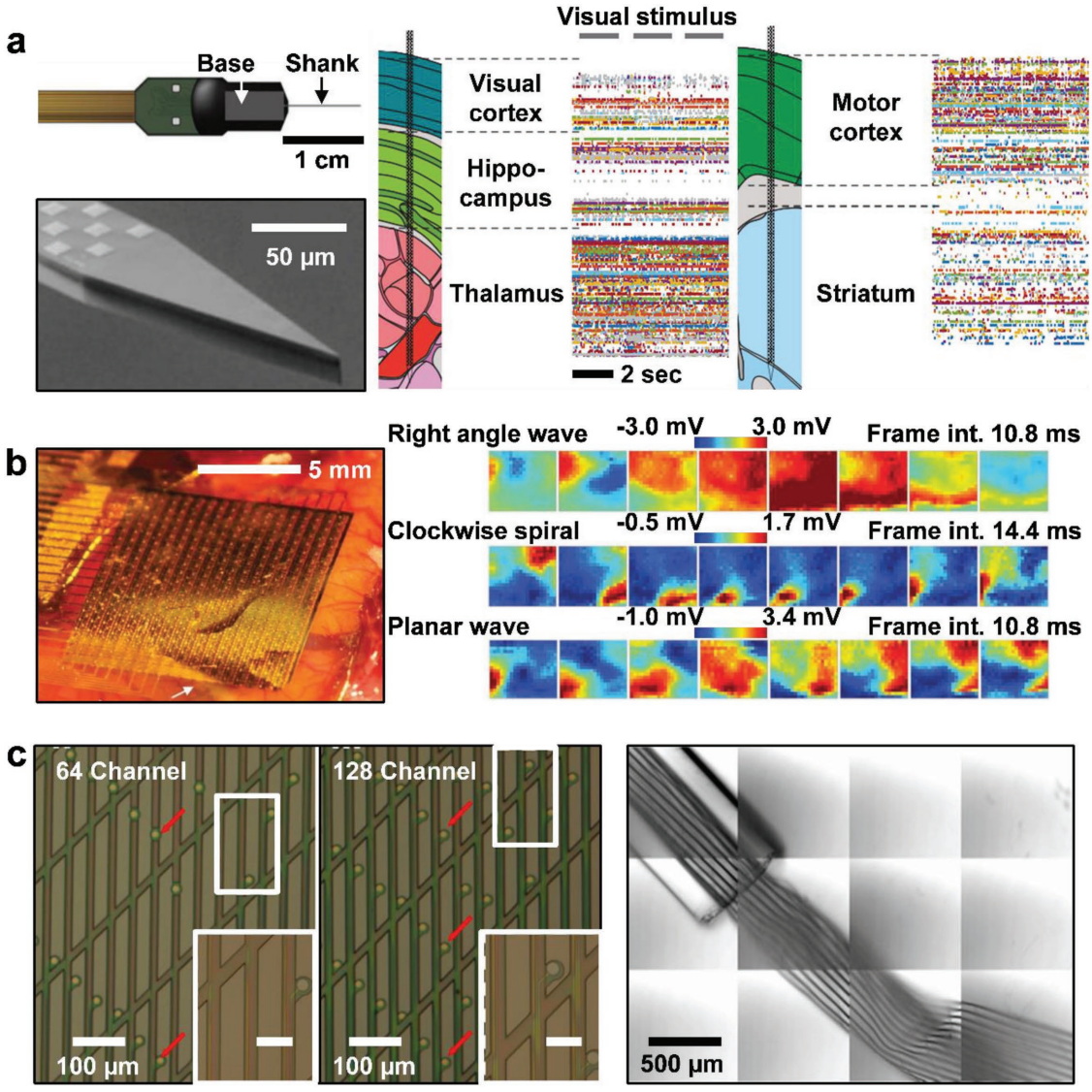

Figure 3. High-density neural interface systems. a) Illustration and scanning electron microscope image of a multichannel neural interface system on a nontapered shank. The integrated circuitry for amplification, multiplexing, and digitization in the base allows transmission of noise-free digital data from the probe (left). Such probes in the brain of an awake mouse simultaneously capture activity from 740 individual neurons across diverse regions of brain (right). Reproduced with permission.[136] Copyright 2017, Nature Publishing Group. b) Photograph of actively multiplexed flexible electronics placed on the cortical surface of a feline model (left). Movie frames show recorded spatial temporal, 2D µECoG data during the labeled time interval (right). Reproduced with permission.[53] Copyright 2011, Nature Publishing Group. c) Optical image of 64-channel (left) and 128-channel mesh (middle) electronics probes. The inset shows zoom-in view of isolatedly addressable recording sites (left). Scale bar: 50 µm. Glass syringe with 400 µm inner diameter delivers the mesh electronics into the water (right). Reproduced with permission.[145] Copyright 2017, National Academy of Sciences.

sites (pitch of 25 μm) use TiN electrodes for low impedance (≈150 kΩ at 1 kHz, area of ≈210 μm^2) performance. The probe packaging scheme (left) includes a sensory shank and a head stage for bidirectional data transmission. Here, modern integrated circuit technology provides essential capabilities in high-speed, high-fidelity signal acquisition. Results (right) from chronic (150 d) operation in the brain of an awake mouse include recording from 740 isolated single neurons across five structures of the brain: visual cortex, hippocampus, thalamus, motor cortex, and striatum.

Mechanically flexible systems with similar capabilities in active electronics are of interest for their ability to establish interfaces to curved, dynamic, soft biological systems over areas or volumes rather than just along narrow strips.[138–144] Si NMs, when combined with thin substrates and other supporting materials, enable this level of functionality, thereby allowing high-density electrophysiological mapping from cortical surfaces and other challenging tissue surfaces. Implementation involves integration of Si NM transistors with passive electrodes through techniques of transfer printing (Figure 3b).[53] One such system involves 360 sensing channels in architectures that provide active matrix addressing and per-channel amplification, with capabilities in establishing conformal contact over large, curvilinear surfaces of the cerebral cortex (left) for mapping performance comparable to that of the best systems built on rigid, planar silicon wafers. The movie frames (right) correspond to snapshots of spatiotemporal recordings of electrophysiology associated with sleep spindles, visual evoked responses, and seizures in a feline model. The interface electrodes (pitch of ≈500 μm) consist of layers of Pt (50 nm thick) to achieve a low impedance (≈ 20 kΩ at 1 kHz, area of 9×10^4 μm^2) interface. Scaled versions of this platform with enhanced spatial resolution allow for studies of the auditory cortex.[137]

Removing selected regions of these systems between the electrode sites yields open mesh structures with further enhanced mechanics, as described in the previous section. An example of a high-density passive system (64 channels (left) and 128 channels (middle)) with this type of architecture appears in Figure 3c;[145] the red arrows (left) identify Pt microelectrodes. A related mesh structure (right) enables scalable, multichannel operation with ultrathin substrates (≈400 nm) of photodefined epoxy (SU-8). Such designs maintain ultracompliant mechanics and minimal electrical crosstalk between channels. Demonstration experiments indicate possibilities for injection through a syringe (diameter of 400 μm), for recording local field potentials from individual neurons in various regions of the brain, for up to 4 months.

3.2. Flexible Encapsulation Materials for Chronic Operation

A daunting challenge in the use of platforms that embed active electronics, as opposed to passive interconnects, is that penetration of biofluids can lead to harmful leakage currents into the adjacent tissues and to degradation of the electronics.[146–151] A critical challenge, then, in active neural interfaces is in thin, flexible encapsulation layers that can serve as a biocompatible, defect-free barrier to biofluids with lifetimes measured in decades or more.

These encapsulation materials must prevent biofluid penetration from both the front and back sides of the systems and must be available in thin film geometries with sufficient flexibility.[146] Popular organic (i.e., SU-8, parylene C, polyimide, and PDMS) and inorganic (i.e., SiN_x Al_2O_3, and HfO_2) passivation materials show some promise,[88,113,152–154] but generally fail to offer perfect barrier properties when fully immersed in warm biofluids for decades.[149] Silicon carbide is another promising encapsulation material[155–158] based on reported in vitro and in vivo results. Systematic studies are needed to establish relevant reaction models, water diffusivity, and stability in electrolyte solution for long time durations. Other conventional coatings formed by spin casting, physical vapor deposition, CVD, and atomic layer deposition (ALD), particularly when performed in academic cleanroom settings, cannot meet requirements for defect densities (0 across the entire area of the device, typically between 1 and 10 cm^{-2}). A recently developed alternative exploits physically transferred layers of silicon dioxide (SiO_2) formed by thermal growth on the polished surfaces of silicon wafers. The result is a class of thin film encapsulation that is free of defects over macroscopic areas (up to the sizes of the wafers) even at sub-micrometer thicknesses, with negligible water permeation, excellent biocompatibility, and projected survivability of many decades in buffered saline solutions at physiological conditions. **Figure 4**a presents a series of colorized cross-sectional scanning electron microscope (SEM) images of a 1 μm thick layer of thermal SiO_2 (t-SiO_2) at various time points after immersion in PBS solution at a pH of 7.4 and a temperature of 96 °C.[149] The fundamental limit in lifetime is set not by defects or water permeation, but by a slow hydrolysis reaction ($SiO_2 + 2H_2O \rightarrow Si(OH)_4$) that consumes the material at a dissolution rate of ≈ 90 nm per day at these elevated temperatures. Results of soak testing that involves thin films of magnesium (Mg) encapsulated by such materials appear in Figure 4b.[151] The strong reactivity of Mg with water ($Mg + 2H_2O \rightarrow Mg(OH)_2 + H_2$) rapidly leads to defects upon contact with water, for easy visualization by optical microscopy. Measurements using this approach and others establish that the relationship between the dissolution rate of t-SiO_2 and temperature (Figure 4c) is consistent with Arrhenius scaling with an activation energy of $E_A = 1.32$ eV. The results suggest a dissolution rate of ≈0.04 nm per day at 37 °C PBS solution (pH of 7.4), thereby allowing a 1 μm thick SiO_2 layer to survive for several decades (≈15 nm per year).[149]

By comparison to encapsulation layers formed using other materials deposited by other techniques (e.g., hafnium oxide by atomic layer deposition, Pt by electron-beam deposition, parylene C by CVD, etc.), t-SiO_2 displays superior performance due to its extremely low water permeability and absence of defects. Other candidate materials for barrier layers, including various organic and inorganic chemistries in single and multilayer stacks, fail to match the performance of t-SiO_2 due to water permeation through the materials themselves and/or through pinholes and other forms of defects that can be challenging or impossible to avoid, particularly in academic research environments. t-SiO_2 fails, however, to block transport of ions (e.g., Na^+, K^+, and others present in biofluids) driven by electrical biases associated with operation of the underlying electronics.[150] Ion accumulation at interfaces can alter the operation of

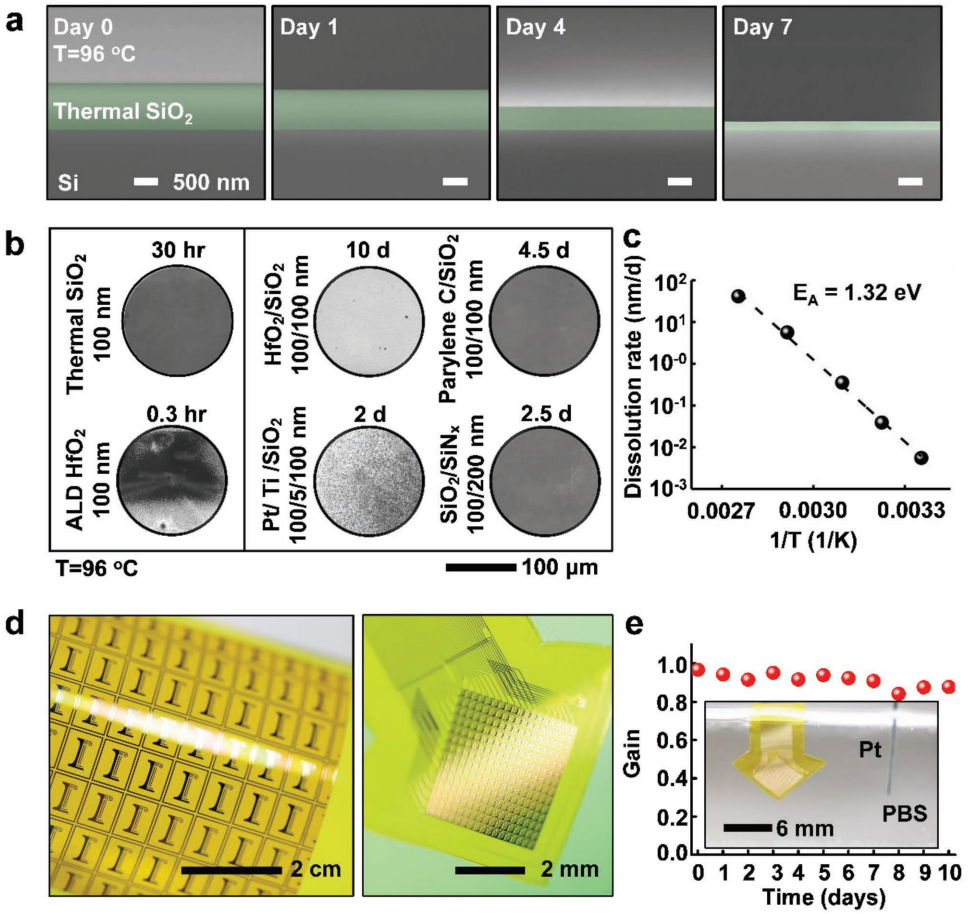

Figure 4. Flexible encapsulation materials for chronic operation. a) Series of images showing dissolution of a layer of SiO_2 (1 µm) soaked in PBS solution at 96 °C. b) Dissolution of Mg encapsulated by a bilayer of t-SiO_2 (100 nm) and HfO_2 (100 nm) (left), and double layer by various capping material, including HfO_2, parylene C, Pt, and SiN_x on a bilayer of SiO_2 (100 nm) (right). Reproduced with permission.[151] Copyright 2017, Wiley-VCH Verlag. c) Dissolution rate of t-SiO_2 at different temperatures. d) Optical image of an array of patterns of Mg (left) and active matrix (right) encapsulated by a layer of t-SiO_2 with thicknesses of 100 nm and 1000 nm, respectively. e) Accelerated immersion tests (PBS solution at 70 °C) with in vitro measurement of active transistor electrode gain. Reproduced with permission.[149] Copyright 2016, National Academy of Sciences.

transistors due to field-induced shifts in threshold voltage and other effects. Bilayer strategies that combine t-SiO_2 with other materials, such as hafnium oxide formed by ALD, eliminate this shortcoming and also reduce the rates of hydrolysis of the t-SiO_2.[151] The addition of silicon nitride (SiN_x) formed by CVD as an ion barrier is another effective option.[150,159]

Figure 4d demonstrates the use of t-SiO_2 as an encapsulation/dielectric layer for electrophysiology mapping devices that operate via capacitive coupling.[146,149] Unlike a conventional fabrication sequence in which deposition of the encapsulation material occurs as a final step on fully formed devices, here the process occurs in the opposite order, with electronics fabricated on top of a preformed layer of t-SiO_2. Specifically, semiconductor processing on the SiO_2/Si wafer yields high-performance electronics and interface electrodes, where the SiO_2 ultimately serves as the encapsulation and/or a dielectric layer for capacitively coupled sensing. Laminating a thin film of polyimide on top of this system and then removing the wafer represent the final steps in forming flexible, high-performance electronics encapsulated with defect-free layers of dense t-SiO_2. Transfer printing an additional layer of t-SiO_2 released from a separate Si wafer onto the bare surface of the polyimide prevents biofluid penetration from the backside. Figure 4d shows pictures of devices encapsulated in this manner, including test platforms with an array of patterns of Mg (in the form of the "I" logo for the University of Illinois) (left) and systems with actively multiplexed electronics (right).[149] In this case, a collection of Si NM transistors (Figure 4e) interface to 252 separate sensing sites, in a layout with 14 columns by 18 rows. The t-SiO_2 extends across the entire system to prevent biofluid penetration at all locations. Figure 4e demonstrates stable and uniform transistor gain values (measured from the multiplexed array in Figure 4d, right) throughout 10 d of immersion in PBS solution at 70 °C (pH of 7.4), as displayed in the inset of Figure 4e.[149] By Arrhenius scaling, these results suggest lifetimes of at least several decades at 37 °C.

Other reports demonstrate that thin foils of stainless steel can also serve as effective encapsulation materials.[160–162] Foils with thicknesses of 50 µm can provide perfect encapsulation in PBS solution (pH of 7.4) at 96 °C for several months.[149] Such foils cannot, however, be used as capacitive or optical interfaces

and they cannot be rendered into films with sub-micrometer thickness for low bending stiffness.

3.3. Bioresorbable Interfaces

Developing materials and other supporting technologies, such as those described in the previous sections, for long-lived electronic neural interfaces represents a frontier direction for materials science. Another emerging focus of work emphasizes the opposite extreme, i.e., devices that function for a certain period of time, typically days or weeks, and then disappear entirely via processes of bioresorption. Application opportunities include diagnostic or therapeutic systems that provide high-performance, stable operation on timescales that match transient processes such as healing or neuroregeneration. Bioresorption then serves as a mechanism to eliminate the devices from the body after the function is no longer necessary, thereby avoiding the need for secondary surgical extraction procedures.

Such systems must exploit collections of materials that are fundamentally different from those outlined in previous sections. Recent work reveals that device technologies based on Si NMs as interface electrodes and as active semiconductor materials can provide the basis of bioresorbable neural interfaces for recording/stimulation with multiplexing/amplification, when integrated with bioresorbable metals (e.g., Mg, Zinc (Zn), molybdenum (Mo), W, etc.), dielectrics (e.g., SiO_2, magnesium oxide (MgO), SiNx, etc.), and thin substrates (e.g., poly(lactic-*co*-glycolic) acid (PLGA), collagen, silk fibroin, etc.) (**Figure 5**a).[60] The fabrication methods combine lithographic processing with

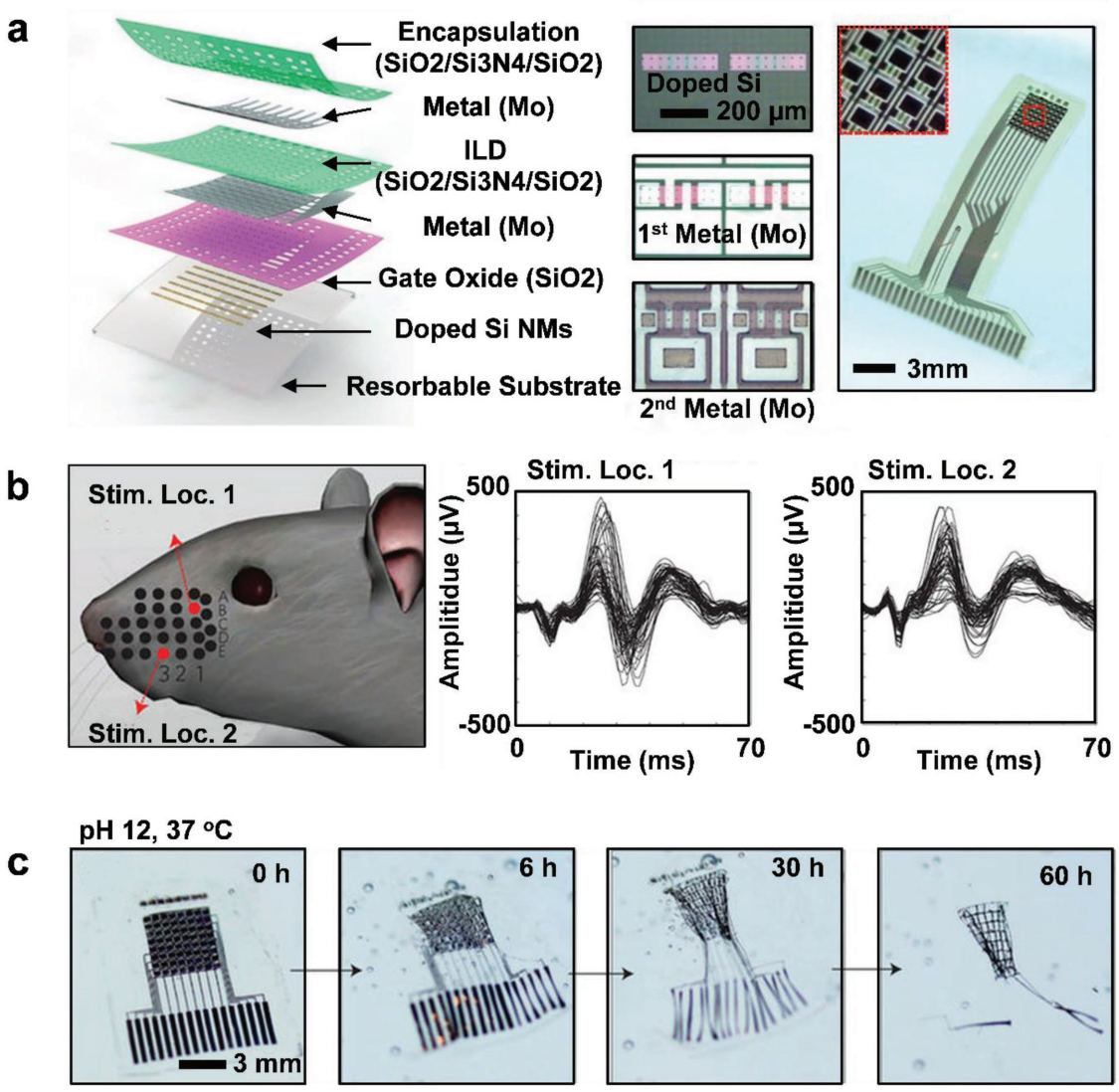

Figure 5. Bioresorbable neural interfaces. a) Schematic exploded-view illustration of a multiplexed neural interface system constructed entirely with bioresorbable materials (left). Optical image of the fabrication steps and a photograph of a complete bioresorbable, actively multiplexed neural electrode array (right). b) Illustration of the procedure for producing evoked potential by stimulating two different whiskers (left) and corresponding recorded temporal evoked pattern. c) Series of images showing accelerated dissolution of a device soaked in PBS (pH 12) solution at 37 °C. Reproduced with permission.[60] Copyright 2016, Nature Publishing Group.

techniques in materials growth and transfer printing to yield thin, flexible mapping arrays with active electronics (left). Briefly, the process (right) begins with formation of Si-NM metal-oxide-semiconductor field-effect transistors (MOSFETs) and Si NM neural interface electrodes. Photolithographically patterned metallization (Mo, 300 nm thick) serves as source, drain, and gate electrodes. A trilayer of $SiO_2/Si_3N_4/SiO_2$ encapsulates the front side, with openings to electrode pads of Mo. The resultant systems enable capabilities in high-resolution neural recording, as shown in Figure 5b for the case of a rat model. Here, responses associated with somatosensory evoked potential experiments (left) appear with high signal-to-noise ratio. The corresponding result (center, right) shows temporally resolved patterns induced by the evoked potentials. Figure 5c summarizes accelerated dissolution tests associated with immersion in PBS solution at 37 °C and a pH of 12. At simulated physiological conditions, the dissolution occurs in a layer-by-layer fashion, starting with the encapsulation stack (SiO_2/Si_3N_4) over ≈6 months at 37 °C PBS solution (pH of 7.4). The Mo sensing electrodes dissolve at a rate of ≈16–25 nm per day under the same condition. The PLGA substrate and the underlying transistor arrays dissolve over several months, with biocompatible end products.[159,163–166] These and other bioresorbable materials provide the basis of broad capabilities in temporary neural interfaces, with many application possibilities that complement those of traditional devices.

3.4. Optoelectronic Interfaces

Most of the technologies described in the previous sections can be used for both neural modulation and recording. Although electrical stimulation represents a standard means to activate neurons[7,167,168] in neuroscience research and in various clinical treatments for disorders such as Parkinson disease,[169–171] tremors,[172] and many of forms of depression,[173] parasitic heating and other undesired effects, together with the lack of cellular specificity, represent significant limitations.[173] Recent progress establishes capabilities for genetically modifying certain populations of neurons in a way that creates sensitivity to light via optically active ion channels or proteins. The results allow optical stimulation or inhibition of neural activity.[174–177] Hardware advances for providing programmed illumination at the neural interface rely critically on advanced materials and unusual device designs. One set of activities in this area focuses on ultrathin, flexible, and wireless optoelectronic implants in geometries similar to the Michigan probes and shanks described previously but with designs capable of activating regions of interest through the use of cellular-scale light-emitting diodes (microscale inorganic light-emitting diodes or μ-ILEDs).[113,178] **Figure 6**a shows such a system mounted on a thin, needle-shaped flexible polymer support.[178] The light-emitting components are microscale light-emitting diodes formed using high-quality, epitaxially grown gallium nitride (GaN), lithographically patterned, and then released from an underlying growth substrate. Stacked integration of additional electronic components and sensors, including ultrathin silicon photodiodes based on Si NMs, electrodes, and temperature sensors allows multifunctional operation. The overall wireless systems, including the light sources, detectors, sensors, and other components, bond onto releasable, injection microneedles (lateral dimension of 300 μm) to facilitate insertion into brain tissue.[178]

Near- or far-field electromagnetic coupling enables battery-free operation and wireless control. Devices that leverage near field communication (NFC) technology operate via magnetic coupling at a frequency of 13.56 MHz and provide a versatile option that is compatible with most neuroscience studies. The schematic illustration in Figure 6b (the top parallel) shows a platform that includes an μ-ILED (blue emission) at the tip of a freely adjustable needle for optogenetic activation in the deep brain and another separate μ-ILED located subdermally as a visual indicator (red emission).[179] The images of Figure 6b show such a device in a bent form (left), with a stretched serpentine connection (right). Insertion into the brain and other areas (Figure 6c), scheme (top) and photograph (bottom)), such as the spinal cord and various parts of the peripheral nervous system is possible,[180] with stable operation for more than a year. Recently developed wireless devices also include multimodal sensors for physiological measurements and microfluidic systems for pharmacological delivery, as reviewed in elsewhere.[181]

Transparent neural electrodes are important in this context because they allow electrophysiological recording and optogenetic activation, with simultaneous imaging of biological responses such as morphological changes, collagen formation, immune responses, or development of scar tissues, directly under the electrode surfaces.[182] In one example, graphene serves as the electrode material in an electrode array (Figure 6d) with transparency greater than 90% from the ultraviolet to the infrared region of the spectrum.[183] Demonstration experiments illustrate possibilities in multimodal operation on the somatosensory cortex of mouse models, with a blue laser (λ = 473 nm) to deliver optogenetic stimuli to neurons directly below the electrode (left). The graphene electrodes in this example have impedances of 240 kΩ at 1 kHz (area of 4×10^4 μm^2), comparable to Pt electrodes (190 kΩ at 1 kHz) with similar dimensions. Experiments allow recordings of evoked potentials from light stimulus (1.24–24.4 mW mm^{-2}) and imaging of the cortical vasculature through optical coherence tomography (right). In separate but related work, graphene electrodes on ultrathin polyimide substrates (thickness of 12.5 μm) yield electrophysiological recordings during calcium imaging by confocal and two-photon microscopy.[184] One challenge with these systems arises from optically induce electrical artifacts, generally smaller in amplitude and temporally different than the light evoked signal, yet still present in a way that can obscure key features of the recordings.[183] Recent efforts suggest that organic electrochemical transistors with PEDOT:PSS as the channel material can suppress such artifacts by compensation of charge traps with highly doped holes in PEDOT:PSS and low site impedances (10 kΩ at 1 kHz, area of 1.4×10^3 μm^2).[62] Figure 6e shows a device that includes both transparent OECTs (PEDOT:PSS with thickness of 150 nm) and transparent metal grid wiring (linewidth of 3 μm) embedded in a parylene substrate (1.2 μm thick) and passivated with a layer of photodefinable epoxy (i.e., SU-8; 1.2 μm thick).[62] The transparency of the device (≈60% transparent for wavelengths

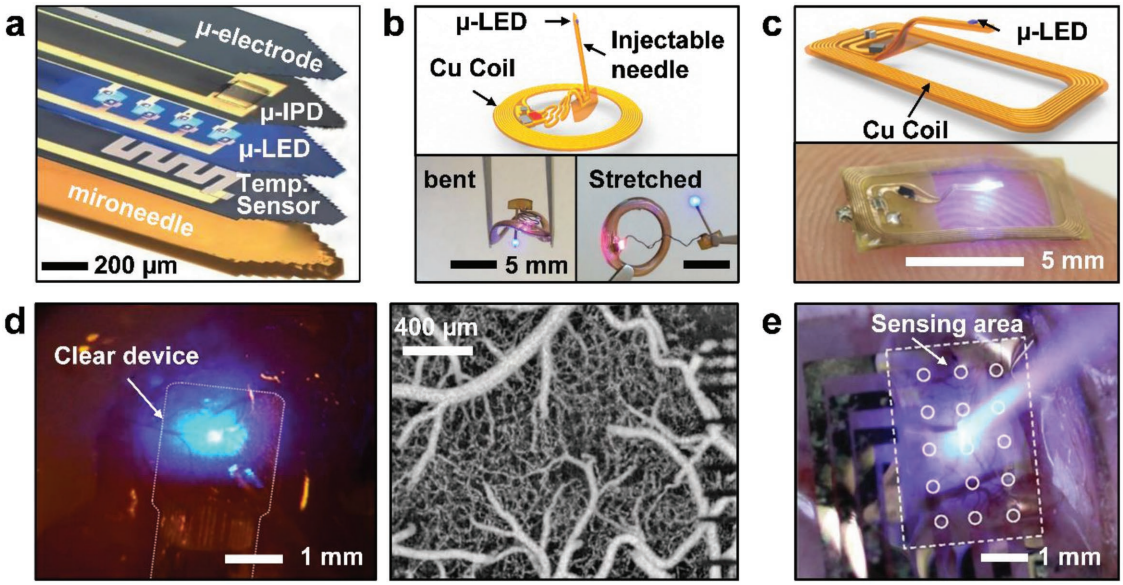

Figure 6. Optoelectronic neural interfaces. a) Schematic exploded-view illustration of a thin, needle-shaped flexible polymer probe for an electrical, optical, and thermal neural interface. Reproduced with permission.[178] Copyright 2013, American Association for the Advancement of Science. b) Schematic illustration of a stretchable, wirelessly powered optogenetic stimulator for application in the deep brain (top). Photograph of the device after bending (left bottom) and stretching (right bottom). Reproduced with permission.[179] Copyright 2017, Cell Press. c) Schematic illustration (top) and photograph (bottom) of an NFC powered optogenetic stimulator for application in the spinal cord. Reproduced with permission.[180] Copyright 2017, Lippincott Williams & Wilkins. d) Photograph of optical stimulation on the somatosensory cortex of mouse model while electrophysiological recording through transparent graphene-based electrode (left). Optical coherence tomography imaging of the cortical vasculature through clear device (right). Reproduced with permission.[183] Copyright 2016, Nature Publishing Group. e) Photograph of OECT-based transparent electrophysiology array on the cortical surface of optogenetic mice during optical stimulation. Reproduced with permission.[62] Copyright 2017, National Academy of Sciences.

from 350 to 800 nm) enables collection of ECoG signals during optical activation (475 nm wavelength), with optical artifacts smaller than the noise level.

4. Conclusions and Perspectives

The results presented here represent some of the most recent materials strategies for neural interface engineering and the resulting systems that are now available. An interrelated collection of advances in material science, mechanical/electrical engineering, and nanoscale fabrication techniques underpins the progress, where large-scale, high-density interfaces capable of multimodal interactions with thousands of neurons with stable chronic operation and minimal foreign-body immune responses can now be achieved. Representative improvements include capabilities for fully implanting electrodes in/on soft tissues for long periods of time, where the constituent materials range from conventional metals, to organic/inorganic hybrids, conducting polymers, graphene, carbon nanotubes, and others. The associated materials strategies and fabrication processes described here may serve as foundations for accelerated rates of progress in electrode performance and scalability. The breakthrough in such systems seems to be accelerating, as momentum builds from previous findings and new strategies emerge. The outcomes promise to enable new, powerful capabilities with significant consequences not only for neuroscience research but also for unusual treatment approaches to neurological disorders and diseases. Parallel efforts in opto- and chemogenetic schemes along with materials and supporting hardware for wireless data transmission, power harvesting, and external control form the foundations of future directions, where integration will ultimately occur not only on surfaces but throughout 3D volumes, from the single neuron level, to neural networks and entire organ systems.

In all cases, however, development of minimally invasive strategies to implant and seamlessly integrate high-performance, high-resolution electronic technologies across large areas of the nervous system for chronic operation remains a grand challenge for the field. Fundamental difficulties are in procedures for deployment and integration, methods for monitoring and perhaps actively modulating biological immune responses over time, and schemes for building soft, deformable systems that conform to complex curvilinear, time-dynamic surfaces but which incorporate ultrathin, long-lived biofluid barriers. Ultimately, such platforms must distribute not only over surfaces but through 3D volumes. This review highlights some progress in each of these directions, but overcoming these challenges will likely require additional, fundamentally new concepts in materials science and engineering, where strategies for geometric expansion and/or transformation may find utility and conducting polymers or hybrid biotic/abiotic composites are likely to play important roles. Stimuli-responsive polymers,[105–107,185,186] impurity-doped diamond,[187–189] and liquid crystal polymers[190] are among the many materials options that could result in further advances.

In addition, advances in signal processing and modulation based on precise data streams could serve as the basis for future

conditional and closed loop technologies. Recent advances in electrode materials integrated with local channel signal processors and optogenetic interfaces to modulate the activity of neurons in highly targeted manner, both reviewed in this article, may be useful in this context. Multimodal operation, distributed architectures with redundant designs and seamless biointegration at the level of materials, mechanics, and geometry seem to be essential features of any envisioned system. Such technologies will have critical roles as advanced tools for research in neuroscience but also as clinical devices for diagnostics, surgical purposes, and, ultimately, as long-term therapeutic systems that can operate as engineered medicines, with value that could complement that of traditional pharmaceutical approaches. The early translation of emerging advances, such as those highlighted in this review, into early commercial medical devices, including all of the appropriate approval processes, will be essential to the support of additional research and resultant iterative cycles of invention and innovation.[6] The diversity of the scientific and engineering content, together with strong consequences of progress for human health/well-being, suggests an exciting future for this field.

Acknowledgements

S.M.W. and E.S. contributed equally to this work. All authors have given approval to the final version of the manuscript. This article is part of the Advanced Materials Hall of Fame article series, which recognizes the excellent contributions of leading researchers to the field of materials science.

Conflict of Interest

The authors declare no conflict of interest.

Keywords

bioelectronics, electrodes, neural interfaces, neural recording, neural stimulation

Received: January 24, 2018
Revised: February 28, 2018
Published online: May 31, 2018

[1] B. S. Appleby, P. S. Duggan, A. Regenberg, P. V. Rabins, *Mov. Disord.* **2007**, *22*, 1722.
[2] R. J. Andrews, *Ann. N. Y. Acad. Sci.* **2003**, *993*, 1.
[3] J. Y. Fang, C. Tolleson, *Neuropsychiatr. Dis. Treat.* **2017**, *13*, 723.
[4] S. M. Wellman, J. R. Eles, K. A. Ludwig, J. P. Seymour, N. J. Michelson, W. E. McFadden, A. L. Vazquez, T. D. Y. Kozai, *Adv. Funct. Mater.* **2018**, *28*, 1701269.
[5] a) A. Branner, R. B. Stein, E. Fernandez, Y. Aoyagi, R. A. Normann, *IEEE Trans. Biomed. Eng.* **2004**, *51*, 146; b) R. J. Vetter, J. C. Williams, J. F. Hetke, E. A. Nunamaker, D. R. Kipke, *IEEE Trans. Biomed. Eng.* **2004**, *51*, 896.
[6] J. Rivnay, H. Wang, L. Fenno, K. Delsseroth, G. G. Mallaras, *Sci. Adv.* **2017**, *3*, e1601649.
[7] S. F. Cogan, *Annu. Rev. Biomed. Eng.* **2008**, *10*, 275.
[8] D. R. Merrill, M. Bikson, J. G. R. Jefferys, *J. Neurosci. Methods* **2005**, *141*, 171.
[9] L.-J. Tang, M.-H. Wang, H.-C. Tian, X.-Y. Kang, W. Hong, J.-Q. Liu, *Micromachines* **2017**, *8*, 281.
[10] M. D. Ferro, N. A. Melosh, *Adv. Funct. Mater.* **2018**, *28*, 1704335.
[11] J.-W. Jeong, G. Shin, S. I. Park, K. J. Yu, L. Xu, J. A. Rogers, *Neuron* **2015**, *86*, 175.
[12] U. A. Aregueta-Robles, A. J. Woolley, L. A. Poole-Warren, N. H. Lovell, R. A. Green, *Front. Neuroeng.* **2014**, *7*, 15.
[13] A. Petrossians, J. J. Whalen, J. D. Weiland, F. Mansfeld, *J. Electrochem. Soc.* **2011**, *158*, D269.
[14] M. Ganji, A. T. Elthakeb, A. Tanaka, V. Gilja, E. Halgren, S. A. Dayeh, *Adv. Funct. Mater.* **2017**, *27*, 1703018.
[15] E. K. Brunton, B. Winther-Jensen, C. Wang, E. B. Yan, S. H. Gooie, A. J. Lowery, R. Rajan, *Front. Neurosci.* **2015**, *9*, 265.
[16] G. Schalk, J. Mellinger, *A Practical Guide to Brain-Computer Interfacing with BCI2000*, Springer, London **2010**, p. 9.
[17] J. Wolpaw, E. Wolpaw, *Brain-Computer Interfaces: Principles and Practice*, Oxford University Press, Oxford **2012**, p. 169.
[18] R. A. Green, P. B. Matteucci, C. W. D. Dodds, J. Palmer, W. F. Dueck, R. T. Hassarati, P. J. Byrnes-Preston, N. H. Lovell, G. J. Suaning, *J. Neural Eng.* **2014**, *11*, 056017.
[19] M. S. Humayun, J. D. Weiland, G. Y. Fujii, R. Greenberg, R. Williamson, J. Little, B. Mech, V. Cimmarusti, G. Van Boemel, G. Dagnelie, E. de Juan, *Vision Res.* **2003**, *43*, 2573.
[20] M. Mahadevappa, J. D. Weiland, D. Yanai, I. Fine, R. J. Greenberg, M. S. Humayun, *IEEE Trans. Neural Syst. Rehabil. Eng.* **2005**, *13*, 201.
[21] K. Wang, C.-C. Liu, D. Durand, *IEEE Trans. Biomed. Eng.* **2009**, *56*, 6.
[22] D. Zhou, E. Greenbaum, *Implantable Neural Prostheses 1 Devices and Applications*, Springer, Dordrecht **2009**, p. 205.
[23] J. Rivnay, S. Inal, B. A. Collins, M. Sessolo, E. Stavrinidou, X. Strakosas, C. Tassone, D. M. Delongchamp, G. G. Malliaras, *Nat. Commun.* **2016**, *7*, 11287.
[24] K. Sun, S. Zhang, P. Li, Y. Xia, X. Zhang, D. Du, F. H. Isikgor, J. Ouyang, *J. Mater. Sci.: Mater. Electron.* **2015**, *26*, 4438.
[25] L. Groenendaal, F. Jonas, D. Freitag, H. Pielartzik, J. R. Reynolds, *Adv. Mater.* **2000**, *12*, 481.
[26] T.-H Le, Y. Kim, H. Yoon, *Polymers* **2017**, *9*, 150.
[27] D.-H. Kim, S. M. Richardson-Burns, J. L. Hendricks, C. Sequera, D. C. Martin, *Adv. Funct. Mater.* **2007**, *17*, 79.
[28] X. Y. Cui, J. Wiler, M. Dzaman, R. A. Altschuler, D. C. Martin, *Biomaterials* **2003**, *24*, 777.
[29] X. Luo, C. L. Weaver, D. D. Zhou, R. Greenberg, X. T. Cui, *Biomaterials* **2011**, *32*, 5551.
[30] C. Boehler, F. Oberueber, S. Schlabach, T. Stieglitz, M. Asplund, *ACS Appl. Mater. Interfaces* **2016**, *9*, 189.
[31] G. A. Snook, P. Kao, A. S. Best, *J. Power Sources* **2011**, *196*, 1.
[32] X. T. Cui, D. D. Zhou, *IEEE Trans. Neural Syst. Rehabil. Eng.* **2007**, *15*, 502.
[33] T. A. Kung, N. B. Langhals, D. C. Martin, P. J. Johnson, P. S. Cederna, M. G. Urbanchek, *Plast. Reconstr. Surg.* **2014**, *133*, 1380.
[34] C. M. Frost, B. Wei, Z. Baghmanli, P. S. Cederna, M. G. Urbanchek, *Plast. Reconstr. Surg.* **2012**, *129*. 933.
[35] L. Quyang, B. Wei, C.-C. Kuo, S. Pathak, B. Farrell, D. C. Martin, *Sci. Adv.* **2017**, *3*, e1600448.
[36] A. V Patil, A. F. Beker, F. G. M. Wiertz, H. A. Heering, G. Coslovich, R. Vlijm, T. H. Oosterkamp, *Nanoscale* **2010**, *2*, 734.
[37] E. W. Keefer, B. R. Botterman, M. I. Romero, A. F. Rossi, G. W. Gross, *Nat. Nanotechnol.* **2008**, *3*, 434.
[38] R.-S. Chen, W.-H. Huang, H. Tong, Z.-L. Wang, J.-K. Cheng, *Anal. Chem.* **2003**, *75*, 6341.
[39] G. H. Kim, K. Kim, H. Nam, K. Shin, W. Choi, J. H. Shin, G. Lim, *Sens. Actuators, B* **2017**, *252*, 152.
[40] F. Vitale, S. R. Summerson, B. Aazhang, C. Kemere, M. Pasquali, *ACS Nano* **2015**, *9*, 4465.

[41] N. Li, X. Zhang, Q. Song, R. Su, Q. Zhang, T. Kong, L. Liu, G. Jin, M. Tang, G. Cheng, *Biomaterials* **2011**, *32*, 9374.
[42] D. Sahni, A. Jea, J. A. Mata, D. C. Marcano, *J. Neurosurg. Pediatr.* **2013**, *11*, 575.
[43] S. Gurunathan, J.-H. Kim, *Int. J. Nanomed.* **2016**, *11*, 1927.
[44] X. Guo, N. Mei, *J. Food Drug Anal.* **2014**, *22*, 105.
[45] M. Xu, J. Zhu, F. Wang, Y. Xiong, Y. Wu, Q. Wang, J. Weng, Z. Zhang, W. Chen, S. Liu, *ACS Nano* **2016**, *10*, 3267.
[46] M. Nurunnabi, Z. Khatun, K. M. Huh, S. Y. Park, D. Y. Lee, K. J. Cho, Y.-K. Lee, *ACS Nano* **2013**, *7*, 6858.
[47] K. Yang, J. Wan, S. Zhang, Y. Zhang, S.-T. Lee, Z. Liu, *ACS Nano* **2011**, *5*, 516.
[48] K. Yang, H. Gong, X. Shi, J. Wan, Y. Zhang, Z. Liu, *Biomaterials* **2013**, *34*, 2787.
[49] K. Wang, J. Ruan, H. Song, J. Zhang, Y. Wo, S. Guo, D. Cui, *Nanoscale Res. Lett.* **2011**, *6*, 1.
[50] K. Kostarelos, M. Vincent, C. Hebert, J. Garrido, *Adv. Mater.* **2017**, *29*, 1700909.
[51] Y. Lu, H. Lyu, A. G. Richardson, T. H. Lucas, D. Kuzum, *Sci. Rep.* **2016**, *6*, 33526.
[52] C.-W. Wang, C.-Y. Pan, H.-C. Wu, P.-Y. Shih, C.-C. Tsai, K.-T. Liao, L.-L. Lu, W.-H. Hsieh, C.-D. Chen, Y.-T. Chen, *Small* **2007**, *3*, 1350.
[53] J. Viventi, D.-H. Kim, L. Vigeland, E. S. Frechette, J. A. Blanco, Y. S. Kim, A. E. Avrin, V. R. Tiruvadi, S.-W. Hwang, A. C. Vanleer, D. F. Wulsin, K. Davis, C. E. Gelber, L. Palmer, J. Van der Spiegel, J. Wu, J. Xiao, Y. Huang, D. Contreras, J. A. Rogers, B. Litt, *Nat. Neurosci.* **2011**, *14*, 1599.
[54] C. M. Lopez, J. Putzeys, B. C. Raducanu, M. Ballini, S. Wang, A. Andrei, V. Rochus, R. Vandebriel, S. Severi, C. Van Hoof, S. Musa, N. Van Helleputte, R. F. Yazicioglu, S. Mitra, *IEEE Trans. Biomed. Circuits Syst.* **2017**, *11*, 510.
[55] B. M. Blaschke, N. Tort-Colet, A. Guimerà-Brunet, J. Weinert, L. Rousseau, A. Heimann, S. Drieschner, O. Kempski, R. Villa, M. V. Sanchez-Vives, J. A. Garrido, *2D Mater.* **2017**, *4*, 025040.
[56] F. Veliev, Z. Han, D. Kalita, A. Briançon-Marjollet, V. Bouchiat, C. Delacour, *Front. Neurosci.* **2017**, *11*, 466.
[57] F. Patolsky, B. P. Timko, G. Yu, Y. Fang, A. B. Greytak, G. Zheng, C. M. Lieber, *Science* **2006**, *313*, 1100.
[58] B. Z. Tian, T. Cohen-Karni, Q. Qing, X. J. Duan, P. Xie, C. M. Lieber, *Science* **2010**, *329*, 830.
[59] W. Zhou, X. Dai, C. M. Lieber, *Rep. Prog. Phys.* **2017**, *80*, 016701.
[60] K. J. Yu, D. Kuzum, S.-W. Hwang, B. H. Kim, H. Juul, N. H. Kim, S. M. Won, K. Chiang, M. Trumpis, A. G. Richardson, H. Cheng, H. Fang, M. Thompson, H. Bink, D. Talos, K. J. Seo, H. N. Lee, S.-K. Kang, J.-H. Kim, J. Y. Lee, Y. Huang, F. E. Jensen, M. A. Dichter, T. H. Lucas, J. Viventi, B. Litt, J. A. Rogers, *Nat. Mater.* **2016**, *15*, 782.
[61] D. Khodagholy, T. Doublet, P. Quilichini, M. Gurfinkel, P. Leleux, A. Ghestem, E. Ismailova, T. Hervé, S. Sanaur, C. Bernard, G. G. Malliaras, *Nat. Commun.* **2013**, *4*, 1575.
[62] W. Lee, D. Kim, N. Matsuhisa, M. Nagase, M. Sekino, G. G. Malliaras, T. Yokota, T. Someya, *Proc. Natl. Acad. Sci. USA* **2017**, *114*, 10554.
[63] B. Tian, J. Liu, T. Dvir, L. Jin, J. H. Tsui, Q. Qing, Z. Suo, R. Langer, D. S. Kohane, C. M. Lieber, *Nat. Mater.* **2012**, *11*, 986.
[64] J. Liu, T.-M. Fu, Z. Cheng, G. Hong, T. Zhou, L. Jin, M. Duvvuri, Z. Jiang, P. Kruskal, C. Xie, Z. Suo, Y. Fang, C. M. Lieber, *Nat. Nanotechnol.* **2015**, *10*, 629.
[65] C. Xie, J. Liu, T.-M. Fu, X. Dai, W. Zhou, C. M. Lieber, *Nat. Mater.* **2015**, *14*, 1286.
[66] H. Zhang, J. Shih, J. Zhu, N. A. Kotov, *Nano Lett.* **2012**, *12*, 3391.
[67] Z. J. Du, X. Luo, C. L. Weaver, X. T. Cui, *J. Mater. Chem. C* **2015**, *3*, 6515.
[68] H. Zhang, W. H. Pei, S. S. Zhao, X. W. Yang, R. C. Liu, Y. Y. Liu, X. Wu, D. M. Guo, Q. Gui, X. H. Guo, X. Xing, Y. J. Wang, H. D. Chen, *Sci. China: Technol. Sci.* **2016**, *59*, 1399.
[69] Y. H. Kim, A. Y. Kim, G. H. Kim, Y. H. Han, M.-A. Chung, S.-D. Jung, *Biomed. Microdevices* **2016**, *18*, 14.
[70] C. Zhang, J.-Q. Liu, H.-C. Tian, X.-Y. Kang, J.-C. Du, Y.-F. Rui, B. Yang, C.-S. Yang, *Microsyst. Technol.* **2015**, *21*, 139.
[71] H.-B. Zhou, G. Li, X.-N. Sun, Z.-H. Zhu, Q.-H. Jin, J.-L. Zhao, Q.-S. Ren, *J. Microelectromech. Syst.* **2009**, *18*, 88.
[72] J. T. Robinson, M. Jorgolli, A. K. Shalek, M.-H. Yoon, R. S. Gertner, H. Park, *Nat. Nanotechnol.* **2012**, *7*, 180.
[73] N. Li, Q. Zhang, S. Gao, Q. Song, R. Huang, L. Wang, L. Liu, J. Dai, M. Tang, G. Cheng, *Sci. Rep.* **2013**, *3*, 1604.
[74] F. Santoro, Y. van de Burgt, S. T. Keene, B. Cui, A. Salleo, *ACS Appl. Mater. Interfaces* **2017**, *9*, 39116.
[75] K. A. Moxon, S. Hallman, A. Aslani, N. M. Kalkhoran, P. I. Lelkes, *J. Biomater. Sci., Polym. Ed.* **2007**, *18*, 1263.
[76] Z. Bérces, K. Tóth, G. Márton, I. Pál, B. Kováts-Megyesi, Z. Fekete, I. Ulbert, A. Pongrácz, *Sci. Rep.* **2016**, *6*, 35944.
[77] A. Rosengren, L. Wallman, N. Danielsen, T. Laurell, L. M. Bjursten, *IEEE Trans. Biomed. Eng.* **2002**, *49*, 392.
[78] Q. L. Loh, C. Choong, *Tissue Eng., Part B* **2013**, *19*, 485.
[79] I. R. Minev, N. Wenger, G. Courtine, S. P. Lacour, *APL Mater.* **2015**, *3*, 014701.
[80] S. Chen, W. Pei, Q. Gui, R. Tang, Y. Chen, S. Zhao, H. Wang, H. Chen, *Sens. Actuators, A* **2013**, *193*, 141.
[81] D. Yoo, J. Kim, J. H. Kim, *Nano Res.* **2014**, *7*, 717.
[82] G. Chan, D. J. Mooney, *Trends Biotechnol.* **2008**, *26*, 382.
[83] S. Sirivisoot, R. Pareta, B. S. Harrison, *Interface Focus* **2014**, *4*, 20130050.
[84] R. A. Green, K. S. Lim, W. C. Henderson, R. T. Hassarati, P. J. Martens, N. H. Lovell, L. A. Poole-Warren, in *2013 35th Ann. Int. Conf. of the IEEE Engineering in Medicine and Biology Society*, IEEE, Osaka, Japan **2013**, p. 6957.
[85] R. T. Hassarati, W. F. Dueck, C. Tasche, P. M. Carter, L. A. Poole-Warren, R. A. Green, *IEEE Trans. Neural Syst. Rehabil. Eng.* **2014**, *22*, 411.
[86] R. A. Green, R. T. Hassarati, J. A. Goding, S. Baek, N. H. Lovell, P. J. Martens, L. A. Poole-Warren, *Macromol. Biosci.* **2012**, *12*, 494.
[87] Y. H. Zhong, X. J. Yu, R. Gilbert, R. V. Bellamkonda, *J. Rehabil. Res.* **2001**, *38*, 627.
[88] C. D. Lee, S. A. Hara, L. Yu, J. T. W. Kuo, B. J. Kim, T. Hoang, V. Pikov, E. Meng, J. Biomed. *Mater. Res., Part B* **2016**, *104*, 357.
[89] W. M. Grill, S. E. Norman, R. V. Bellamkonda, *Annu. Rev. Biomed. Eng.* **2009**, *11*, 1.
[90] P. J. Rousche, R. A. Normann, *IEEE Trans. Rehabil. Eng.* **1999**, *7*, 56.
[91] P. A. House, J. D. MacDonald, P. A. Tresco, R. A. Normann, *Neurosurg. Focus* **2006**, *20*, 1.
[92] H. A. C. Wark, R. Sharma, K. S. Mathews, E. Fernandez, J. Yoo, B. Christensen, P. Tresco, L. Rieth, F. Solzbacher, R. A. Normann, *J. Neural Eng.* **2013**, *10*, 045003.
[93] J. C. Barrese, N. Rao, K. Paroo, C. Triebwasser, C. Vargas-Irwin, L. Franquemont, J. P. Donoghue, *J. Neural Eng.* **2013**, *10*, 066014.
[94] S. Negi, R. Bhandari, L. Rieth, F. Solzbacher, *Biomed. Mater.* **2010**, *5*, 15007.
[95] A. Fujishiro, H. Kaneko, T. Kawashima, M. Ishida, T. Kawano, *Sci. Rep.* **2014**, *4*, 4868.
[96] L. Luan, X. Wei, Z. Zhao, J. J. Siegel, O. Potnis, C. A. Tuppen, S. Lin, S. Kazmi, R. A. Fowler, S. Holloway, *Sci. Adv.* **2017**, *3*, e1601966.
[97] A. Canales, X. Jia, U. P. Froriep, R. A. Koppes, C. M. Tringides, J. Selvidge, C. Lu, C. Hou, L. Wei, Y. Fink, P. Anikeeva, *Nat. Biotechnol.* **2015**, *33*, 277.
[98] H. S. Sohal, A. Jackson, R. Jackson, G. J. Clowry, K. Vassilevski, A. O'Neill, S. N. Baker, *Front. Neuroeng.* **2014**, *7*, 10.

[99] Z. L. Xiang, S.-C. Yen, N. Xue, T. Sun, W. M. Tsang, S. S. Zhang, L.-D. Liao, N. V. Thakor, C. Lee, *J. Micromech. Microeng.* **2014**, *24*, 065015.
[100] T. D. Kozai, D. R. Kipke, *J. Neurosci. Methods* **2009**, *184*, 199.
[101] A. W. Hirschberg, H. Xu, K. Scholten, T. W. Berger, D. Song, E. Meng, in *IEEE 30 Int. Conf. on Micro Electro Mechanical Systems*, IEEE, Las Vegas, NV **2017**, p. 129.
[102] H. Xu, A. W. Hirschberg, K. Scholten, T. W. Berger, D. Song, E. Meng, *J. Neural Eng.* **2018**, *15*, 016017.
[103] I. D. Dryg, M. P. Ward, K. Y. Qing, H. Mei, J. E. Schaffer, P. P. Irazoqui, *IEEE Trans. Neural Syst. Rehabil. Eng.* **2015**, *23*, 562.
[104] J. R. Capadona, D. J. Tyler, C. A. Zorman, S. J. Rowan, C. Weder, *MRS Bull.* **2012**, *37*, 581.
[105] J. R. Capadona, K. Shanmuganathan, D. J. Tyler, S. J. Rowan, C. Weder, *Science* **2008**, *319*, 1370.
[106] T. Ware, D. Simon, C. Liu, T. Musa, S. Vasudevan, A. Sloan, E. W. Keefer, R. L. RennakerII, W. Voit, *J. Biomed. Mater. Res., Part B* **2014**, *102*, 1.
[107] T. Ware, D. Simon, R. L. Rennaker, W. Voit, *Polym. Rev.* **2013**, *53*, 108.
[108] A. J. Shoffstall, S. Srinivasan, M. Willis, A. M. Stiller, M. Ecker, W. E. Voit, J. J. Pancrazio, J. R. Capadona, *Sci. Rep.* **2018**, *8*, 122.
[109] D. M. Simon, H. Charkhkar, C. St. John, S. Rajendran, T. Kang, R. Reit, D. Arreaga-Salas, D. G. Mchail, G. L. Knaack, A. Sloan, D. Grasse, T. C. Dumas, R. L. Rennaker, J. J. Pancrazio, W. E. Voit, *J. Biomed. Mater. Res., Part A* **2017**, *105*, 159.
[110] W. H. Kang, W. Cao, S. Wagner, B. Morrison, in *Stretchable Electronics* (Ed: T. Someya), Wiley-VCH Verlag GmbH & Co. KGaA, Weinheim, Germany **2012**, p. 379.
[111] P. V. Bayly, T. S. Cohen, E. P. Leister, D. Ajo, E. C. Leuthardt, G. M. Genin, *J. Neurotrauma* **2005**, *22*, 845.
[112] K. S. Topp, B. S. Boyd, *Phys. Ther.* **2006**, *86*, 92.
[113] S. I. Park, D. S. Brenner, G. Shin, C. D. Morgan, B. A. Copits, H. U. Chung, M. Y. Pullen, K. N. Noh, S. Davidson, S. J. Oh, J. Yoon, K.-I. Jang, V. K. Samineni, M. Norman, J. G. Grajales-Reyes, S. K. Vogt, S. S. Sundaram, K. M. Wilson, J. S. Ha, R. Xu, T. Pan, T.-I. Kim, Y. Huang, M. C. Montana, J. P. Golden, M. R. Bruchas, R. W. Gereau, J. A. Rogers, *Nat. Biotechnol.* **2015**, *33*, 1280.
[114] K.-I. Jang, K. Li, H. U. Chung, S. Xu, H. N. Jung, Y. Yang, J. W. Kwak, H. H. Jung, J. Song, C. Yang, A. Wang, Z. Liu, J. Y. Lee, B. H. Kim, J.-H. Kim, J. Lee, Y. Yu, B. J. Kim, H. Jang, K. J. Yu, J. Kim, J. W. Lee, J.-W. Jeong, Y. M. Song, Y. Huang, Y. Zhang, J. A. Rogers, *Nat. Commun.* **2017**, *8*, 15894.
[115] I. R. Minev, P. Musienko, A. Hirsch, Q. Barraud, N. Wenger, E. M. Moraud, J. Gandar, M. Capogrosso, T. Milekovic, L. Asboth, R. F. Torres, N. Vachicouras, Q. Liu, N. Pavlova, S. Duis, A. Larmagnac, J. Voeroes, S. Micera, Z. Suo, G. Courtine, S. P. Lacour, *Science* **2015**, *347*, 159.
[116] D. Khodagholy, J. N. Gelinas, T. Thesen, W. Doyle, O. Devinsky, G. G. Malliaras, G. Buzsaki, *Nat. Neurosci.* **2015**, *18*, 310.
[117] D.-H. Kim, J. Viventi, J. J. Amsden, J. Xiao, L. Vigeland, Y. S. Kim, J. A. Blanco, B. Panilaitis, E. S. Frechette, D. Contreras, D. L. Kaplan, F. G. Omenetto, Y. Huang, K. C. Hwang, M. R. Zakin, B. Litt, J. A. Rogers, *Nat. Mater.* **2010**, *9*, 511.
[118] S. Choi, H. Lee, R. Ghaffari, T. Hyeon, D.-H. Kim, *Adv. Mater.* **2016**, *28*, 4203.
[119] W. M. Choi, J. Song, D. Y. Khang, H. Jiang, Y. Y. Huang, J. A. Rogers, *Nano Lett.* **2007**, *7*, 1655.
[120] M. Kaltenbrunner, T. Sekitani, J. Reeder, T. Yokota, K. Kuribara, T. Tokuhara, M. Drack, R. Schwodiauer, I. Graz, S. Bauer-Gogonea, S. Bauer, T. Someya, *Nature* **2013**, *499*, 458.
[121] J. Zang, S. Ryu, N. Pugno, Q. Wang, Q. Tu, M. J. Buehler, X. Zhao, *Nat. Mater.* **2013**, *12*, 321.
[122] D.-H. Kim, W. M. Choi, J. H. Ahn, H.-S. Kim, J. Song, Y. Y. Huang, Z. Liu, C. Lu, C. G. Koh, J. A. Rogers, *Appl. Phys. Lett.* **2008**, *93*, 044102.
[123] Z. Yan, M. Han, Y. Shi, A. Badea, Y. Yang, A. Kulkarni, E. Hanson, M. E. Kandel, X. Wen, F. Zhang, Y. Luo, Q. Lin, H. Zhang, X. Guo, Y. Huang, K. Nan, S. Jia, A. W. Oraham, M. B. Mevis, J. Kim, X. Guo, M. Gao, W. Ryu, K. J. Yu, B. G. Nicolau, A. Petronico, S. S. Rubakhin, J. Lou, P. M. Ajayan, K. Thornton, G. Popescu, D. Fang, J. V. Sweedler, P. V. Braun, H. Zhang, R. G. Nuzzo, Y. Huang, Y. Zhang, J. A. Rogers, *Proc. Natl. Acad. Sci. USA* **2017**, *114*, E9455.
[124] R. Feiner, L. Engel, S. Fleischer, M. Malki, I. Gal, A. Shapira, Y. Shacham-Diamand, T. Dvir, *Nat. Mater.* **2016**, *15*, 679.
[125] T. J. Oxley, N. L. Opie, S. E. John, G. S. Rind, S. M. Ronayne, T. L. Wheeler, J. W. Judy, A. J. McDonald, A. Dornom, T. J. H. Lovell, C. Steward, D. J. Garrett, B. A. Moffat, E. H. Lui, N. Yassi, B. C. V. Campbell, Y. T. Wong, K. E. Fox, E. S. Nurse, I. E. Bennett, S. H. Bauquier, K. A. Liyanage, N. R. van der Nagel, P. Perucca, A. Ahnood, K. P. Gill, B. Yan, L. Churilov, C. R. French, P. M. Desmond, M. K. Horne, L. Kiers, S. Prawer, S. M. Davis, A. N. Burkitt, P. J. Mitchell, D. B. Grayden, C. N. May, T. J. O'Brien, *Nat. Biotechnol.* **2016**, *34*, 320.
[126] R. K. Sefcik, N. L. Opie, S. E. John, C. P. Kellner, J. Mocco, T. J. Oxley, *Neurosurg. Focus* **2016**, *40*, E7.
[127] N. L. Opie, S. E. John, G. S. Rind, S. M. Ronayne, D. B. Grayden, A. N. Burkitt, C. N. May, T. J. O'Brien, T. J. Oxley, *J. Neural Eng.* **2016**, *13*, 046020.
[128] D. K. Freeman, J. M. O'Brien, P. Kumar, B. Daniels, R. A. Irion, L. Shraytah, B. K. Ingersoll, A. P. Magyar, A. Czarnecki, J. Wheeler, J. R. Coppeta, M. P. Abban, R. Gatzke, S. I. Fried, S. W. Lee, A. E. Duwel, J. J. Bernstein, A. S. Widge, A. Hernandez-Reynoso, A. Kanneganti, M. I. Romero-Ortega, S. F. Cogan, *Front. Neurosci.* **2017**, *11*, 659.
[129] D. Seo, R. M. Neely, K. Shen, U. Singhal, E. Alon, J. M. Rabaey, J. M. Carmena, M. M. Maharbiz, *Neuron* **2016**, *91*, 529
[130] W. J. Freeman, L. J. Rogers, M. D. Holmes, D. L. Silbergeld, *J. Neurosci. Methods* **2000**, *95*, 111.
[131] M. W. Slutzky, L. R. Jordan, T. Krieg, M. Chen, D. J. Mogul, L. E. Miller, *J. Neural Eng.* **2010**, *7*, 26004.
[132] D. Khodagholy, J. N. Gelinas, Z. Zhao, M. Yeh, M. Long, J. D. Greenlee, W. Doyle, O. Devinsky, G. Buzsáki, *Sci. Adv.* **2016**, *2*, e1601027
[133] T. Castermans, M. Duvinage, G. Cheron, T. Dutoit, *Brain Sci.* **2014**, *4*, 1.
[134] L. F. Nicolas-Alonso, J. Gomez-Gil, *Sensors* **2012**, *12*, 1211.
[135] I. H. Stevenson, K. P. Kording, *Nat. Neurosci.* **2011**, *14*, 139.
[136] J. J. Jun, N. A. Steinmetz, J. H. Siegle, D. J. Denman, M. Bauza, B. Barbarits, A. K. Lee, C. A. Anastassiou, A. Andrei, Ç. Aydın, M. Barbic, T. J. Blanche, V. Bonin, J. Couto, B. Dutta, S. L. Gratiy, D. A. Gutnisky, M. Häusser, B. Karsh, P. Ledochowitsch, C. M. Lopez, C. Mitelut, S. Musa, M. Okun, M. Pachitariu, J. Putzeys, P. D. Rich, C. Rossant, W. Sun, K. Svoboda, M. Carandini, K. D. Harris, C. Koch, J. O'Keefe, T. D. Harris, *Nature* **2017**, *551*, 232.
[137] M. A. Escabı´, H. L. Read, J. Viventi, D.-H. Kim, N. C. Higgins, D. A. Storace, A. S. Liu, A. M. Gifford, J. F. Burke, M. Campisi, Y.-S. Kim, A. E. Avrin, J. V. Spiegel, Y. Huang, M. Li, J. Wu, J. A. Rogers, B. Litt, Y. E. Cohen, *J. Neurophysiol.* **2014**, *112*, 1566.
[138] D.-H. Kim, N. Lu, R. Ma, Y.-S. Kim, R.-H. Kim, S. Wang, J. Wu, S. M. Won, H. Tao, A. Islam, K. J. Yu, T.-I. Kim, R. Chowdhury, M. Ying, L. Xu, M. Li, H.-J. Chung, H. Keum, M. McCormick, P. Liu, Y.-W. Zhang, F. G. Omenetto, Y. Huang, T. Coleman, J. A. Rogers, *Science* **2011**, *333*, 838.
[139] D.J. Lipomi, M. Vosgueritchian, B. C.-K. Tee, S. L. Hellstrom, J. A. Lee, C. H. Fox, Z. Bao, *Nat. Nanotechnol.* **2011**, *6*, 788.

[140] M. C. McAlpine, H. Ahmad, D. Wang, J. R. Heath, *Nat. Mater.* **2007**, *6*, 379.
[141] W. Gao, S. Emaminejad, H. Y. Y. Nyein, S. Challa, K. Chen, A. Peck, H. M. Fahad, H. Ota, H. Shiraki, D. Kiriya, D.-H. Lien, G. A. Brooks, R. W. Davis, A. Javey, *Nature* **2016**, *529*, 509.
[142] W. Wu, L. Wang, Y. Li, F. Zhang, L. Lin, S. Niu, D. Chenet, X. Zhang, Y. Hao, T. F. Heinz, J. Hone, Z. L. Wang, *Nature* **2014**, *514*, 470.
[143] S. Xu, Y. Zhang, L. Jia, K. E. Mathewson, K.-I. Jang, J. Kim, H. Fu, X. Huang, P. Chava, R. Wang, S. Bhole, L. Wang, Y. J. Na, Y. Guan, M. Flavin, Z. Han, Y. Huang, J. A. Rogers, *Science* **2014**, *344*, 70.
[144] C. M. Lochner, Y. Khan, A. Pierre, A. C. Arias, *Nat. Commun.* **2014**, *5*, 5745.
[145] T. M. Fu, G. Hong, R. D. Viveros, T. Zhou, C. M. Lieber, *Proc. Natl. Acad. Sci. USA* **2017**, *114*, E10046.
[146] H. Fang, K. J. Yu, C. Gloschat, Z. Yang, E. Song, C. Chiang, J. Zhao, S. Won, S. Xu, M. Trumpis, Y. Zhong, S. W. Han, Y. Xue, D. Xu, S. W. Choi, G. Cauwenberghs, M. Kay, Y. Huang, J. Viventi, I. R. Efimov, J. A. Rogers, *Nat. Biomed. Eng.* **2017**, *1*, 38.
[147] M. M. Laks, R. Arzbaecher, J. J. Bailey, D. B. Gaselowitz, A. S. Berson, *Circulation* **1996**, *93*, 837.
[148] C. D. Swerdlow, W. H. Olson, M. E. O'Connor, D. M. Gallik, R. A. Malkin, M. Laks, *Circulation* **1999**, *99*, 2559.
[149] H. Fang, J. Zhao, K. J. Yu, E. Song, A. B. Farimani, C.-H. Chiange, X. Jin, Y. Xue, D. Xu, W. Dui, K. J. Seo, Y. Zhong, Z. Yang, S. M. Won, G. Fang, S. W. Choi, S. Chaudhuri, Y. Huang, M. A. Alam, J. Viventi, N. R. Aluru, J. A. Rogers, *Proc. Natl. Acad. Sci. USA* **2016**, *113*, 11682.
[150] E. Song, H. Fang, X. Jin, J. Zhao, C. Jiang, K. J. Yu, Y. Zhong, D. Xu, J. Li, G. Fang, H. Du, J. Zhang, J. M. Park, Y. Huang, M. A. Alam, Y. Mei, J. A. Rogers, *Adv. Electron. Mater.* **2017**, *3*, 1700077.
[151] E. Song, Y. K. Lee, R. Li, J. Li, X. Jin, K. J. Yu, Z. Xie, H. Fang, Y. Zhong, H. Du, J. Zhang, G. Fang, Y. Kim, Y. Yoon, M. A. Alam, Y. Mei, Y. Huang, J. A. Rogers, *Adv. Funct. Mater.* **2017**, *28*, 1702284.
[152] X. Xie, L. Rieth, L. Williams, S. Negi, R. Bhandari, R. Caldwell, R. Sharma, P. Tathireddy, F. Solzbacher, *J. Neural Eng.* **2014**, *11*, 026016.
[153] B. Branch, J. L. Schei, G. Gupta, A. M. Dattelbaum, D. N. Petsev, J. S. Geroge, *IEEE Sens. J.* **2015**, *15*, 4992.
[154] S. Wurth, M. Capogrosso, S. Raspopovic, J. Gandar, G. Federici, N. Kinany, A. Cutrone, A. Piersigilli, N. Pavlova, R. Guiet, G. Taverni, J. Rigosa, P. Shkorbatova, X. Navarro, Q. Barraud, G. Courtine, S. Micera, *Biometerials* **2017**, *122*, 114.
[155] F. Deku, Y. Cohen, A. Joshi-Imre, A. Kanneganti, T. J. Gardner, S. F. Cogan, *J. Neural Eng.* **2018**, *15*, 016007.
[156] G. L. Knaack, D. G. Mchail, G. Borda, B. S. Koo, N. Peixoto, S. F. Cogan, T. C. Dumas, J. J. Pancrazio, *Front. Neurosci.* **2016**, *10*, 301.
[157] X. Lei, S. Kane, S. Cogan, H. Lorach, L. Galambos, P. Huie, K. Mathieson, T. Kamins, J. Harris, D. Palanker, *J. Neural Eng.* **2016**, *13*, 46016.
[158] S. F. Cogan, D. J. Edell, A. A. Guzelian, Y. Ping Liu, R. Edell, *J. Biomed Mater. Res., Part A* **2003**, *67*, 856.
[159] S.-K. Kang, S.-W. Hwang, H. Cheng, S. Yu, B. H. Kim, J.-H. Kim, Y. Huang, J. A. Rogers, *Adv. Funct. Mater.* **2014**, *24*, 4427.
[160] M.-H. Park, J.-Y. Kim, T.-H. Han, T.-S. Kim, H. Kim, T.-W. Lee, *Adv. Mater.* **2015**, *27*, 4308.
[161] C.-H. Chen, J.-T. Gau, R.-S. Lee, *Mater. Manuf. Processes* **2009**, *24*, 1256.
[162] Z. Wu, L. Wang, C. Chang, Y. Qiu, *J. Phys. D: Appl. Phys.* **2005**, *38*, 981.
[163] S.-W. Hwang, H. Tao, D.-H. Kim, H. Cheng, J. K. Song, E. Rill, M. A. Brenckle, B. Panilaitis, S. M. Won, Y.-S. Kim, Y. M. Song, K. J. Yu, A. Ameen, R. Li, Y. Su, M. Yang, D. L. Kaplan, M. R. Zakin, M. J. Slepian, Y. Huang, F. G. Omenetto, J. A. Rogers, *Science* **2012**, *337*, 1640.
[164] L. Yin, H. Cheng, S. Mao, R. Haasch, Y. Liu, X. Xie, S.-W. Hwang, H. Jain, S.-K. Kang, Y. Su, R. Li, Y. Huang, J. A. Rogers, *Adv. Funct. Mater.* **2014**, *24*, 645.
[165] S.-K. Kang, S.-W. Hwang, S. Yu, J. H. Seo, E. A. Corbin, J. Shin, D. S. Wie, R. Bashir, Z. Ma, J. A. Rogers, *Adv. Funct. Mater.* **2015**, *25*, 1789.
[166] S.-W. Hwang, D.-H. Kim, H. Tao, T.-I. Kim, S. Kim, K. J. Yu, B. Panilaitis, J.-W. Jeong, J.-K. Song, F. G. Omenetto, J. A. Rogers, *Adv. Funct. Mater.* **2013**, *23*, 4087.
[167] P. K. Campbell, K. E. Jones, R. J. Huber, K. W. Horch, R. A. Normann, *IEEE Trans. Biomed. Eng.* **1991**, *38*, 758.
[168] T. D. Kozai, N. B. Langhals, P. R. Patel, X. Deng, H. Zhang, K. L. Smith, J. Lahann, N. A. Kotov, D. R. Kipke, *Nat. Mater.* **2012**, *11*, 1065.
[169] R. G. Bittar, S. C Burn, P. G. Bain, S. L. Owen, C. Joint, D. Shlugman, T. Z. Aziz, *J. Clin. Neurosci.* **2005**, *12*, 457.
[170] P. Krack, A. Batir, N. Van Blercom, S. Chabardes, V. Fraix, C. Ardouin, A. Koudsie, P. D. Limousin, A. Benazzouz, J. F. LeBas, A. L. Benabid, *N. Eng. J. Med.* **2003**, *349*, 1925.
[171] J. S. Perlmutter, J. W. Mink, *Annu. Rev. Neurosci.* **2006**, *29*, 229.
[172] W. C. Koller, K. E. Lyons, S. B. Wilkinson, R. Pahwa, *Mov. Disord.* **1999**, *14*, 847.
[173] H. S. Mayberg, A. M. Lozano, V. Voon, H. E. McNeely, D. Seminowicz, C. Hamani, J. M. Schwalb, S. H. Kenney, *Neuron* **2005**, *45*, 651.
[174] M. L. Kringelbach, N. Jenkinson, S. L. F. Owen, T. Z. Aziz, *Nat. Rev. Neurosci.* **2007**, *8*, 623.
[175] R. P. Bonin, F. Wang, M. Desrochers-Couture1, A. Ga secka, M. E. Boulanger, D. C. Côté, Y. De Koninck, *Mol. Pain* **2016**, *12*, 1.
[176] C. Towne, K. L. Montgomery, S. M. Iyer, K. Deisseroth, S. L. Delp, *PLoS One* **2013**, *8*, e72691.
[177] S. M. Iyer, K. L. Montgomery, C. Towne, S. Y. Lee, C. Ramakrishnan, K. Deisseroth, S. L. Delp, *Nat. Biotechnol.* **2014**, *32*, 274.
[178] T.-I. Kim, J. G. McCall, Y. H. Jung, X. Huang, E. R. Siuda, Y. Li, J. Song, Y. M. Song, H. A. Pao, R.-H. Kim, C. Lu, S. D. Lee, I.-S. Song, G. Shin, R. Al-Hasani, S. Kim, M. P. Tan, Y. Huang, F. G. Omenetto, J. A. Rogers, *Science* **2013**, *340*, 211.
[179] G. Shin, A. M. Gomez, R. Al-Hasani, Y. R. Jeong, J. Kim, Z. Xie, A. Banks, S. M. Lee, S. Y. Han, C. J. Yoo, J.-L. Lee, S. H. Lee, J. Kurniawan, J. Tureb, Z. Guo, J. Yoon, S.-I. Park, S. Y. Bang, Y. Nam, M. C. Walicki, V. K. Samineni, A. D. Mickle, K. Lee, S. Y. Heo, J. G. McCall, T. Pan, L. Wang, X. Feng, T.-I. Kim, J. K. Kim, Y. Li, Y. Huang, R. W. Gereau, J. S. Ha, M. R. Bruchas, J. A. Rogers, *Neuron* **2017**, *93*, 509.
[180] V. K. Saminenia, J. Yoon, K. E. Crawford, Y. R. Jeong, K. C. Mckenzie, G. Shin, Z. Xie, S. S. Sundaram, Y. Li, M. Y. Yang, J. Kim, D. Wu, Y. Xue, X. Feng, Y. Huang, A. D. Mickle, A. Banks, J. S. Ha, J. P. Golden, J. A. Rogers, R. W. Gereau, *Pain* **2017**, *158*, 2108.
[181] P. Gutruf, J. A. Rogers, *Neurobiology* **2018**, *50*, 1.
[182] D.-W. Park, S. K. Brodnick, J. P. Ness, F. Atry, L. Krugner-Higby, A. Sandberg, S. Mikael, T. J. Richner, J. Novello, H. Kim, D.-H. Baek, J. Bong, S. T. Frye, S. Thongpang, K. I. Swanson, W. Lake, R. Pashaie, J. C. Williams, Z. Ma, *Nat. Protoc.* **2016**, *11*, 2201.
[183] D.-W. Park, A. A. Schendel, S. Mikael, S. K. Brodnick, T. J. Richner, J. P. Ness, M. R. Hayat, F. Atry, S. T. Frye, R. Pashaie, S. Thongpang, Z. Ma, J. C. Williams, *Nat. Commun.* **2014**, *5*, 5258.

[184] D. Kuzum, H. Takano, E. Shim, J. C. Reed, H. Juul, A. G. Richardson, J. de Vries, H. Bink, M. A. Dichter, T. H. Lucas, D. A. Coulter, E. Cubukcu, B. Litt, *Nat. Commun.* **2014**, *5*, 5259.

[185] T. Ware, D. Simon, K. Hearon, C. Liu, S. Shah, J. Reeder, N. Khodaparast, M. P. Kilgard, D. J. Maitland, R. L. Rennaker II, W. E. Voit, *Macromol. Mater. Eng.* **2012**, *297*, 1193.

[186] T. Ware, D. Simon, D. E. Arreaga-Salas, J. Reeder, R. Rennaker, E. W. Keefer, W. Voit, *Adv. Funct. Mater.* **2012**, *22*, 3470.

[187] G. Piret, C. Héber, J.-P Mazellier, L. Rousseau, E. Scorsone, M. Cottance, G. Lissorgues, M. O. Heuschkel, S. Picaud, P. Bergonzo, B. Yvert, *Biomaterials* **2015**, *53*, 173.

[188] H.-Y. Chan, D. M. Aslam, J. A. Wiler, B. Casey, *J. Microelectromech. Syst.* **2009**, *18*, 511.

[189] D. J. Garrett, A. L. Saunders, C. Mcgowan, J. Specks, K. Ganesan, H. Meffin, R. A. Williams, D. A.X. Nayagam, *J. Biomed. Mater. Res., Part B* **2016**, *104*, 19.

[190] T. M. Gwon, C. Kim, S. Shin, J. H. Park, J. H. Kim, S. J. Kim, *Biomed. Eng. Lett.* **2016**, *6*, 148.